Article:
Ali, MY, Fairhead, JD, Green, CM orcid.org/0000-0001-9644-4949 et al. (1 more author) (2017) Basement structure of the United Arab Emirates derived from an analysis of regional gravity and aeromagnetic database. Tectonophysics, 712-71. pp. 503-522. ISSN 0040-1951

https://doi.org/10.1016/j.tecto.2017.06.006

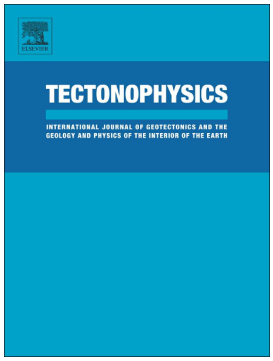

Basement structure of the United Arab Emirates derived from an analysis of regional gravity and aeromagnetic database

M.Y. Ali, J.D. Fairhead, C.M. Green, A. Noufal

PII: S0040-1951(17)30252-4
DOI: doi: 10.1016/j.tecto.2017.06.006
Reference: TECTO 127518

To appear in: *Tectonophysics*

Received date: 23 February 2017
Revised date: 16 May 2017
Accepted date: 6 June 2017

Please cite this article as: M.Y. Ali, J.D. Fairhead, C.M. Green, A. Noufal , Basement structure of the United Arab Emirates derived from an analysis of regional gravity and aeromagnetic database, *Tectonophysics* (2017), doi: 10.1016/j.tecto.2017.06.006

Basement structure of the United Arab Emirates derived from an analysis of regional gravity and aeromagnetic database

M.Y. Ali[1], J.D. Fairhead[2&3], C.M. Green[3] and A. Noufal[4]

[1]The Petroleum Institute, P O Box 2533, Abu Dhabi, UAE, email: mali@pi.ac.ae

[2]JD GEOconsultancy Ltd, Leeds, UK; email: jamesderekfairhead@gmail.com

[3]School of Earth and Environment, University of Leeds, Leeds LS2 9JT, UK; C.M.Green@leeds.ac.uk

[4]ADNOC, P O Box 898, Abu Dhabi, UAE; awnoufal@adnoc.ae

ABSTRACT

Gravity and aeromagnetic data covering the whole territory of the United Arab Emirates (UAE) have been used to evaluate both shallow and deep geological structures, in particular the depth to basement since it is not imaged by seismic data anywhere within the UAE. Thus, the aim has been to map the basement so that its structure can help to assess its control on the distribution of hydrocarbons within the UAE. Power spectrum analysis reveals gravity and magnetic signatures to have some similarities, in having two main density/susceptibility interfaces widely separated in depth such that regional-residual anomaly separation could effectively be undertaken. The upper density/susceptibility interface occurs at a depth of about 1.5 km while the deeper interface varies in depth throughout the UAE. For gravity, this deeper interface is assumed to be due to the combined effect of lateral changes in density structures within the sediments and in depth of basement while for magnetics it is assumed the sediments have negligible susceptibility and the anomalies unrelated to the volcanic/magmatic bodies result from only changes in depth to basement. The power

spectrum analysis over the suspect volcanic/magmatic bodies indicates they occur at ~5 km depth. The finite tilt-depth and finite local wavenumber methods were used to estimate depth to source and only depths that agree to within 10% of each other were used to generate the depth to basement map. This depth to basement map, to the west of the UAE-Oman Mountains, varies in depth from 5 km to in excess of 15 km depth and is able to structurally account for the location of the shear structures, seen in the residual magnetic data, and the location of the volcanic/magmatic centres relative to a set of elongate N-S to NE-SW trending basement highs. The majority of oilfields in the UAE are located within these basement highs. Therefore, the hydrocarbon distribution in the UAE basin appears to be controlled by the location of the basement ridges.

Keywords: basement structure, United Arab Emirates, power spectrum, finite tilt-depth, finite local wavenumber

1. INTRODUCTION

Gravity and magnetic data have been used to delineate crustal structures and flexural rigidity (Ali and Watts, 2009; Karner and Watts, 1983; Ravaut et al., 1997; Stewart and Watts, 1997), tectonic boundaries (Jallouli et al., 2002; King and Barr, 2004; Manghnani and Coleman, 1981; Shelton, 1990; White et al., 2005) and also basement and sedimentary structures (Benson and Floyd, 2000; Khattab, 1995; Salem and Ali, 2016; Warsi, 1990). Gravity and magnetic data are important in locating features that are seismically less easy to recognize such as strike-slip faults, regional discontinuities, dykes and basement surface.

Few gravity and magnetic studies (e.g. Ali et al., 2014; Khattab, 1995; Salem and Ali, 2016) have investigated the crustal and basement structures of the United Arab Emirates (UAE). However, identification of the structural framework of the basement is critical to hydrocarbon exploration of the UAE sedimentary basins. For example, the basement structures may propagate into the overlying sedimentary rocks and influence fluid flow and the distribution of hydrocarbon traps. In addition, the basement structures are formed by tectonic processes that generally control the basin architecture and influence source rock distribution, heat flow, trap timing and sediment supply.

Khattab (1995) suggested that the depth to the pre-Permian basement in the southern Arabian Gulf is around 8.5 km. He assumed that the lineaments derived from gravity and magnetic data are correlated to the strike-slip basement faults in the Zagros fold zone in south eastern Iran. Ali et al. (2014) identified three major structural provinces (fold-and-thrust belt, foreland and salt tectonic provinces) based on the residual Bouguer gravity anomaly. In

addition, Ali et al. (2014) mapped extensive arrays of N-S, NW-SE and NE-SW trending lineaments affecting the basement in the UAE. More recently, Salem and Ali (2016) identified two well-defined positive magnetic anomalies that trend in the NE–SW direction in the north western offshore of Abu Dhabi using high-resolution aeromagnetic data. These anomalies were interpreted to be intra-basement blocks with an average depth of around 8.5 km.

In this study, we compiled all available gravity and aeromagnetic data in the UAE to delineate basement structures that control hydrocarbon traps and structures of the UAE-Oman Mountain belt. To achieve this, it was necessary to identify and remove shallow structures and determine to what extent the gravity images intermediate depth sedimentary structures. In so doing we have developed a method to quality control the depths derived using phase methods (tilt-depth and local wavenumber) so that only solutions that are consistent between these methods are accepted. In addition, seismic data and surface geology were used to constrain the interpretation of the potential field data.

2. GEOLOGICAL SETTING

The UAE is situated in the northeast of the Arabian Peninsula between the Arabian Gulf and the Gulf of Oman (Figure 1). Basement terrains in the UAE are neither exposed nor imaged by available seismic and well data due to the thick sedimentary cover. The deepest well in the UAE was drilled in the Shah field and possibly reached the Sharawra Formation of Silurian age at a depth of 6,609 m (Bloch, 2000).

The basement of eastern Arabia was involved in the Neoproterozoic compressional event

(from c. 715 to 610 Ma) of island-arc and micro-continent terrain accretion that led to the amalgamation and formation of the Arabian margin of Gondwana (Al-Husseini, 2000; Loosveld et al., 1996; Sharland et al., 2001). The consolidation created a pronounced N–S structural fabric of sinistral shear zones in the crust of the Arabian Plate. This basement is assumed to be magnetic basement and is imaged by the regional magnetic survey data and is unconformably overlain by more than 10 km of Late Neoproterozoic to Phanerozoic volcanic and sedimentary sequences, including thick Infracambrian salts.

In the Neoproterozoic to Late Devonian (c. 610 to 364 Ma) period, the Arabian Plate was located in an intracratonic setting within the continental interior of northeastern Gondwana bordering the Palaeo-Tethys Ocean (Al-Husseini, 2000). This phase led to the development of a NW–SE shear fracture system (Najd Fault System) and a number of salt basins (Al-Husseini, 2000). In the Late Carboniferous to mid-Permian (364 Ma to 255 Ma) the Arabian Plate was located in a back-arc setting (Ruban et al., 2007). The associated Hercynian events affected the area, creating regional uplift, widespread erosion, and basement lineations along the inherited, mechanically weak Neoproterozoic trends (Konert et al., 2001).

In the Late Permian, the Neo-Tethys began to open between the Cimmerian continental blocks to the north and the north-eastern margin of the Arabian Plate (Glennie et al., 1974; Searle et al., 2004). The opening of the Neo-Tethys involved a multistage rifting which started in the Late Carboniferous-Early Permian with a ‘non-volcanic’ rifting dominated by block faulting (Blendinger et al., 1990). This was followed by a Late Permian rifting event with volcanism and the final continental break-up with volcanism in the Late Triassic-Early Jurassic (Robertson and Searle, 1990). By the Late Permian, a stable carbonate platform was established along the entire NE Arabian Plate margin (Al-Husseini and Matthews, 2010). The

carbonate platform persisted from the Triassic, through the Jurassic to the Early Cretaceous and Aptian–Cenomanian, as the margin subsided slowly due to post-rift thermal subsidence (Ziegler, 2001).

The Semail Ophiolite (Figure 1) was formed within the Oman segment of the Neo-Tethys during the Cenomanian (Warren et al., 2005). The obduction of the Semail Ophiolite and associated thrust sheets caused loading, flexural subsidence and uplift, and partial erosion of the underlying passive margin shelf carbonates (Patton and O'Connor, 1988). Passive margin sedimentation returned during the Late Campanian–Maastrichtian (Nolan et al., 1990). During Late Oligocene–Miocene time, compressional deformation resumed. This deformation is interpreted as the beginning of the Zagros phase of continent–continent collision when the Musandam shelf collided with the central Iran continental block (Ricateau and Riche, 1980).

3. THE POTENTIAL FIELD DATA

3.1 Aeromagnetic Data Compilation

The total magnetic intensity (TMI) aeromagnetic data set used in this study is an integration of the Aero Service 1980 survey and the Sander Geophysics 2007/8 survey provided to the Petroleum Institute by Abu Dhabi National Oil Company (ADNOC). The outlines of the surveys are shown in Figure 2.

The Aero Service survey was carried out over the whole territory of UAE (land and marine) and had 3 barometric altitudes: the majority of the survey was at 518 m above mean sea level

while over the UAE-Oman Mountains the altitude increased to 1,219 m and for the extreme north eastern portion of the survey a small area was flown at 2,133 m. TMI field measurements were made along flight lines in a WNW-ESE direction with line spacing of 2.5 km and perpendicular tie lines (or control lines) at 10 km intervals. Processing included the removal of the International Geomagnetic Reference Field and line intersection adjustments to remove/minimise diurnal changes in the field strength, location errors and altitude differences. Cultural noise, due to man-made structures on Das Island, and the cities of Abu Dhabi, Dubai and Jebel Ali were also removed. The original grid constructed from these data had 0.015° (~1.67 km) cell size.

The Sander Geophysics GPS (Global Positioning System) controlled survey measured a total of 13,809 line km with line spacing of 2 km and tie lines at 10 km. The flight line direction was N040° with tie lines at N130° for most of the survey; along the northern edge a few lines were orientated at N102° and N076°. The flight line altitude was a drape surface with nominal terrain clearance of 250 m (i.e. 250 m above sea level over most of the area). Caesium optically pumped magnetometers were used on the aircraft as well as at an onshore base-station for determining diurnal variations. The sensitivity of the magnetometers was 0.001 nT with sensor noise less than 0.02 nT. The original grid constructed from this data set had 0.5 km cell size.

The Aero Service and Sander survey grids were merged with the upward continuation of the Sander Geophysics survey to 518 m and re-gridding at 1.7 km cell size. This cell size has been used throughout this study.

3.2 Gravity Data Compilation

The gravity data compilation has been fully described by Ali et al. (2014), with updated gravity coverage map shown in Figure 2. Onshore, the data set consists, in the main, of an ADNOC ground survey containing more than 25,000 stations collected by R. H. Ray in the 1940s and 1950s, while offshore, the data set consists, in the main, of an ADNOC airborne survey consisting of 13,804 line km collected by Sander Geophysics. Smaller ground based, shipboard and sea bottom surveys were also integrated (Ali et al., 2014). In addition, data from eastern offshore Qatar (Sohio) that ADNOC traded with Sohio Qatar Petroleum Company are incorporated (Figure 2). The coverage although good is sparse in the marine areas west and east of the Sander Geophysics survey.

4. INITIAL APPRAISAL OF THE DATA

4.1 Aeromagnetic Data

4.1.1 Transformation of the TMI to the DRTP Field

Inspection of the TMI map (Figure 3a) to the west of the UAE-Oman Mountains shows that the main positive anomalies have negative anomalies associated with their northern sides (i.e. on the side closest to the pole). Examples can be found onshore at 54°E, 23.5°N, and offshore within degree square 52°-53°E and 24°-25°N. These dipole anomalies are caused by magnetisation induced by the geomagnetic field within the magnetic bodies. The dipole nature of magnetic anomalies make them more difficult to interpret in terms of geological structure. Thus, an initial process of removing/minimising the Inclination effect is to transform the TMI map to the Differential Reduction to the Pole (DRTP) map (Arkani-Hamed, 2007). This DRTP transform reduces the magnetic anomalies to the pole and corrects

for variation in Inclination and Declination over the study area assuming that all magnetisation is induced. The mean Inclination and Declination values for the centre of the study area (Figure 3a) are 37.16°N and 1.26°E respectively. The extreme values at the northern end (latitude 25.8°N) are I = 39.41°N and D = 1.47°E while the extreme values at the southern end (latitude 22.6°N) are I = 33.69°N and D = 0.97°E.

The DRTP transformation (Figure 3b) has been successful for the anomalies in degree square 52°-53°E and 24°-25°N, making them symmetric, positive in the centre with a broad surrounding negative, and centred over their causative bodies. However, this is not the case for the large anomaly at 54°E, 23.5°N, which is significantly asymmetric after the DRTP operation. This suggests the source of this magnetic anomaly has significance remanence and is volcanic/magmatic in nature.

Despite this isolated problem, we used the DRTP plot (Figure 3b) for all subsequent analysis of the magnetic field since it is assumed that basement rocks are in general inductively magnetised.

4.1.2 Power Spectrum Analysis

Spectral analysis has been shown to be a powerful, but simple means of analysing magnetic map data to estimate depth to top of magnetic sources and determining the wavelength contributions contained in the magnetic map that come from shallow and deep structures so that their respective fields can be separated by filtering and evaluated separately. The method used is based on original studies by Spector and Grant (1970) and Treitel et al. (1971) with practical application given by Hinze et al. (2013).

For a random ensemble of magnetic sources at an average depth to top of (z) from an observation elevation, the power spectrum (PS) is proportional to the amplitude squared and when averaged over all azimuths can be simplified to:

$$PS(K) = Ce^{-4\pi zf} = Ce^{-2zK} \qquad (1)$$

where K is the wavenumber, f is frequency and λ is wavelength such that $K = 2\pi f = 2\pi/\lambda$ and constant C includes field parameters and random magnetic properties. The size and thickness factors of the source body are here considered negligible. The above expression can then be made into a linear equation (y = mx + C) by taking the natural logarithm of both sides

$$\ln[PS(K)] = \ln[C]-2zK \qquad (2)$$

then the slope of the linear equation, m, = 2z.

The merits of the power spectrum method are that, for anomaly sources at a consistent depth, it is less affected by interference due to overlapping anomalies than other depth estimation methods and it is independent of the directional attributes of the magnetisation of the sources (remanence) and directions of the geomagnetic field. As will be shown, the power spectrum method distinguishes several depth sources allowing filtering to be applied to separate shallow from deep source configurations.

The power spectrum method appears to be an ideal method to analyse the UAE aeromagnetic data since a major part of the magnetic spectrum emanates from considerable depth which is likely to be the top surface of the basement and is separated from the weaker, near surface

magnetic effects. This clear separation between shallow and deep sources allows a reliable determination of the break point wavelength that can be used in filter design to remove/suppress the shallow magnetic responses when evaluating the deep basement structures as shown by Phillips (2001) mathematically.

Initial tests of the power spectrum analysis over the sedimentary areas of the UAE show that the depth to top of the deepest ensemble of sources is generally between 10 km and 20 km while the shallow sources are generally between 1.4 and 2.0 km. Working on the basis that the minimum size of the sampling window should be 4 to 6 times the maximum source depth, and since the target of this study is defining and mapping depth and structure of the basement, a window size of 100 km x 100 km was used. The power spectrum examples for the three windows 1, 2 and 4 (Figure 4) are representative and consistent with the windows centred on the black dots in Figure 3b. For window 3 (Figures 3b and 4c), located in northeast UAE over the UAE-Oman Mountains, the magnetic rocks of the Semail Ophiolite are close to the surface and the power spectrum changes markedly.

Power spectrum depth estimates were undertaken for all the 26 windows (shown in Figure 3b) with window locations having 50% overlap and avoiding the UAE-Oman Mountains. The high slopes located on the longer wavelength side of the power spectrum plots (Figure 4) give estimates of the depth to top of magnetic basement, assuming the sediments are non-magnetic. These depth values were found to be from 9.9 km to 22.0 km with an average of 14.6 km. For the shallower surface, the depth to top ranges from 1.0 km to 1.9 km with an average of 1.55 km. The analysis also provides the wavelength break point between the linear parts of the spectrum so that low pass filtering could be applied to isolate the magnetic response effects of the basement. An alternative and more complete approach to separate the

sources fields is by using matched filters (Phillips, 2001). Such an approach was not used here since there is such a good spectral divide between the shallow and deep sources (Figures 4 and 7). The break point has a range from 12 km to 26 km with an average of 15.4 km. However, over the two areas of strong magnetic anomaly response (52°-53.5°E and 24°-25°N and centred on 53°E, 25°N) a third linear segment of the power spectrum is observed (see red line in Figure 4a) giving estimated depths of between 4 km and 5 km. This third linear segment can also be identified in Figures 4b and 4d and suggests that this segment could be volcanic/magmatic in origin with a top surface shallower than the basement depth which is defined by the high slopes located on the longer wavelength side of the power spectrum plots of Figure 4. To isolate the response of the shallower (~1 km depth) structures the wavelength break point needs to be ~10 km (i.e. lower wavelength end of third linear segment shown in red as part of Window 1 in Figure 4a).

A Butterworth low pass filter using a cut-off wavelength of 10 km and order 6 was used to generate the regional magnetic map (Figure 5a) representing the deep basement surface response and the corresponding residual magnetic maps (Figures 5b and 5c) represent near surface geological responses within the upper 1.5 km. The residual magnetic map (Figure 5b) is basically uncontaminated by the volcanic/magmatic bodies (third segment of the PS plot shown in red in Figure 4a) and appears at first sight to be featureless except for the UAE-Oman Mountains anomalies in the northeast. The regional magnetic map (Figure 5a) has been used to map basement structures, while the colour equalised residual magnetic map (Figure 5c), restricted to the sedimentary areas, west of the UAE-Oman Mountains, reveals the subtle shallow structures.

4.2 Gravity Data

4.2.1 Regional Gravity

Based on the analysis of the power spectrum responses, particularly those close to and over the UAE foreland basin (Figure 1) a Butterworth low pass filter using a cut-off wavelength of 25 km was used to generate the regional gravity map (Figure 6a) that images the gravity response of the deep sedimentary structures and basement surface. The residual gravity map (Figure 6b) was derived by removing Figure 6a from the Bouguer anomaly (not shown) and basically images the gravity response of sedimentary structures within the upper 1.5 km.

The regional Bouguer anomaly map (Figure 6a) has similarities to the regional magnetic map (Figure 5a) in terms of the large positive and negative anomalies associated with the UAE-Oman Mountains and their foreland basin whilst the field is generally smooth over the rest of the UAE. The major differences between the gravity and magnetic maps are the cluster of large magnetic anomalies located in the south central onshore area and in the northwest and northeast offshore. These magnetic anomalies are likely to be caused by volcanic/magmatic bodies with the south central onshore anomalies exhibiting remanent magnetism. There appears to be no equivalent gravity response in these locations indicating that the lateral density contrast between the sediments and volcanic/magmatic bodies is relatively small.

4.2.2 Power Spectrum Analysis

The separation of the regional and residual gravity fields was undertaken based on power spectrum analysis. Over sedimentary basins the gravity power spectrum has a range of problems not necessarily encountered by magnetic data. For magnetic data, the sediments are often relatively non-magnetic. This results in a clean undistorted magnetic response from the basement, whereas for gravity data the presence of 3D variations in lithological density and

the presence of carbonate and salt bodies could result potentially in a complex mix of gravitational responses. In such an environment, the gravity response of the basement interface could be highly variable, if there are spatial variations in the density of the deep sediments. Alternatively, the basement gravity response could be fairly uniform if the density variations in the basal sediments are small with the major lithological density changes occurring at shallow depth.

Gravity power spectrum analysis was undertaken for the same four window locations shown in Figure 3b and displayed in Figure 7, as well as at 20 of the 26 point locations shown in Figure 3b to obtain statistical values of depth estimates and break point. To generate the gravity power spectra, the gravity data need to be converted to the vertical gradient, or vertical derivative (VDR), to make them equivalent to the pseudo-magnetic field. This is done by adding 2ln(K) to ln(PS) on the left hand side of the equation given for the magnetic case. In general, the gravity data are well behaved and, like the magnetic data, generate two linear segments.

4.3 Comparison of Aeromagnetic and Gravity Power Spectra

The magnetic and gravity spectra determined for Windows 1 to 4 (Figure 3b) are compared:
Window 1 – Western offshore (Figures 4a and 7a): The area is located in the Arabian Gulf, northwest of Abu Dhabi (box 1, Figure 3b). A number of islands related to salt diapirism (e.g. Arzanah, Das and Zirku) occur in the area. The magnetic signature of the area is characterised by long wavelength (~50 km) magnetic highs. The gravity signature shows major lows which are coincident salt domes and related oilfields. The gravity spectrum estimates the basement to be significantly shallower than the magnetic spectrum. The

magnetic spectrum has a third segment (red dashed line in Figure 4a) probably resulting from volcanic/magmatic rocks at 4 km to 5 km depth but this is not seen in the gravity spectrum.

Window 2 – Western onshore (Figures 4b and 7b): The magnetic and gravity signature of western offshore (box 2, Figure 3b) is generally quiet reflecting the deep sedimentary cover in the area. The gravity spectrum estimates the thickness of sediments to be slightly less than the magnetic spectrum.

Window 3 – UAE-Oman Mountains (Figures 4c and 7c): The UAE-Oman Mountains (box 3, Figure 3b) are dominated by the Semail Ophiolite complex, which is associated with high gravity and magnetic anomalies. The Semail Thrust along the western front of the ophiolite can be easily mapped both from gravity and magnetic data. The eastern boundary of the Semail Ophiolite is characterised by north-south trending anomalies in offshore Fujairah indicating a low-angle normal faulting (Ali et al., 2014). The response of the shallow section for both the gravity and magnetic spectra dominate with the gravity depth being greater than the magnetic depth estimate.

Window 4 – Foreland basin (Figures 4d and 7d): The magnetic and gravity signatures of the foreland basin (box 4, Figure 3b) are considerably smoother than those of the UAE-Oman Mountains. The basin is infilled with low density and low susceptibility marine sediments. The spectral response is similar to Windows 1 and 2, but has considerably greater thickness of sediments.

Gravity spectral analysis has avoided areas of poor gravity coverage (pastel areas in Figure 6a) and all spectra show a clear separation of shallow and deep sources. For the UAE-Oman

Mountains spectra (Window 3) the responses of the shallow depth segments tend to dominate the power spectra and the gravity depth estimates are greater than the magnetic depth estimates. This is most likely due to the presence of shallow high susceptibility oceanic crust and mantle layers (i.e. Semail Ophiolite), giving rise to strong short wavelength magnetic signals seen over the UAE-Oman Mountains in Figure 5b.

Gravity and magnetic power spectra have been computed for the 20 windows centred on black, red and blue dots shown in Figure 3b. They all exhibit a clear spectral divide between the shallow and deep segments with a third intermediate depth segment best seen over the volcanic/magmatic areas based solely on the magnetic data. This third segment is shown as a red dashed line in Figure 4a.

4.3.1 Shallow Segment

The magnetic data give depths that range from 1.0 km to 1.9 km with an average depth of 1.55 km (depths all relative to survey datum of 518 m above mean sea level). In the UAE-Oman Mountains, the sources of the magnetic anomaly are the ophiolite sequence and volcanic or meta-volcanic units in the metamorphic sole. In the foreland area, the magnetic source may be due to detritic material derived from the ophiolite in the UAE-Oman Mountains. The gravity data give depths that range from 0.4 km to 1.5 km with a mean depth of 0.8 km (depths relative to mean surface topography). The residual magnetic and gravity maps (Figures 5b and 6b) thus relate to lateral variations in susceptibility and density at a depth of about 0.9 km +/- 0.2 km within the upper sedimentary layer.

4.3.2 Deep Segment

For the 10 black dots located in the west and northwest of the UAE (Figure 3b), the gravity data give shallower depth estimates (ranging from 4.9 km to 11 km with mean of 8.6) compared to the depths derived from the magnetic data (ranging from 11.7 km to 18.8 km with mean of 15.2 km). Additionally, for the 4 black dots located in the southeast of the UAE (Figure 3b), the gravity gives much shallower depth estimates (ranging from 10.5 km to 18.0 km with mean of 14.4 km) compared to the depths derived from the magnetic data (ranging from 15.9 km to 22.0 km with mean of 19.4 km). However, for the 6 blue dots located in the central part of the UAE (Figure 3b) the gravity data give greater depth estimates (ranging from 13.5 km to 19.6 km with mean of 15.4 km) compared to the depths derived from the magnetic data (ranging from 9.9 km to 13.5 km with mean of 11.5 km). A possible reason for these shallower depths based on the magnetic data could be due to the presence of shallow volcanic/magmatic bodies probably formed either during initial continental rifting in the Late Permian or final continental breakup in the Late Triassic-Early Jurassic (Ali et al., 2013).

Furthermore, there are an additional 6 locations (red dots) shown in Figure 3b where magnetic depth analysis was undertaken but no gravity depth analysis due to the poor data coverage. The regional gravity map (Figure 6a) thus relates to both deep lateral density variations within the sedimentary section and basement while the regional magnetic map (Figure 5a) relates to basement structures and volcanic/magmatic sources that probably extend into the sedimentary section. These regional magnetic and gravity maps (Figures 5a and 6a) will be used to help map structural lineaments within both the deep sedimentary section and basement.

4.3.3 Intermediate Segment

The intermediate magnetic power spectrum segment (denoted as red line in Figure 4a) could represent the presence of volcanic/magmatic centres with enhanced amplitude with respect to the background field and in one case asymmetric dipole anomalies after DRTP (see Figures 3a and 3b). To analyse the distribution of such centres the Analytic Signal of the DRTP has been constructed (not shown) and using THDR (total horizontal derivative) the outlines of the largest centres have been defined in the central UAE (see section 5.1.5).

5. STRUCTURAL MAPPING

The structural maps constructed in this section are based solely on the gravity and magnetic data sets derived from the regional-residual separation shown in Figures 5 and 6. The basement is considered to have been reactivated at various times (see section 2) which has been reflected in various ways in the overlying sedimentary structures. As such, identifying lineaments and features in the shallow sedimentary section, as defined by the residual gravity and magnetic maps, may in some way relate to the structures that reside in the deeper sedimentary section imaged by the regional gravity map and ultimately to the basement structures imaged by the regional magnetic data. The structural mapping section is thus considered from shallow to deep.

5.1 Shallow Structural Mapping Within the Upper 1.5 km of the Surface

The main structural feature seen in both the residual magnetic and gravity maps (Figures 5b and 6b) is the UAE-Oman Mountains in northeast UAE and their western boundary shown as a thick solid black line. These include west-directed imbricate thrust systems associated with the foreland fold and thrust belt west of the UAE-Oman Mountain belt. Elsewhere, the

residual magnetic map appears at first sight featureless while the residual gravity map contains numerous small amplitude structural trends and circular anomaly lows. These residual anomaly fields are investigated separately below using a range of derivative methods.

There are a number of derivative methods that can be used to enhance the imaging of structural edges; these include standard or traditional derivatives of the DRTP field (THDR; VDR; and Analytic Signal). These derivatives are now supplemented by a range of new local phase derivatives of the DRTP field (Tilt angle, θ; Theta, cos θ; and local wavenumber, K). The amplitudes of the standard gravity and magnetic derivatives, are directly controlled by the lateral variation in density and susceptibility of the source bodies making up the geology, which contributes to the complex process of structural mapping. The new range of phase derivatives are independent of density and susceptibility and more clearly respond to structural and depth changes.

The phase derivatives used in this study are:

5.1.1 Tilt Angle, θ

$$\theta = \tan^{-1}(\mathrm{VDR}/\mathrm{THDR}) \qquad (3)$$

where θ has a value in the range +/- π/2 radians (or +/- 90^0).

This function acts like an automatic gain control balancing the VDR of the field by the THDR within an arctangent function that limits the value of θ to +/- 90^0. The Tilt angle is independent of density or susceptibility since the ratio VDR/THDR cancels out this

parameter. Thus, this derivative is ideal for evaluating structure and depth when sub-surface density and/or susceptibility are highly variable. Assuming vertical contacts and vertical magnetisation (i.e. effective DRTP), the zero Tilt angle contour tracks structural edges and the positive component of the derivative is associated with the positive density or susceptibility contrast side of the contact (Verduzco et al., 2004). The Tilt angle is also used to estimate depth using a method known as tilt-depth (Salem et al., 2007).

5.1.2 Theta Map (or cos θ)

The Theta map converts the zero contour of the Tilt angle to a maximum of 1 which provides an alternative means of tracking structural edges. A limitation of these derivatives is that contours are continuous and close on themselves whereas faults are lineaments with finite length. Thus it is necessary to use a combination of standard derivatives, e.g. THDR and phase derivatives to map fault and contact edges (Fairhead, 2016).

5.1.3 Local Wavenumber, K

The local wavenumber represents the spatial rate of change of local phase (Phillips, 2000; Thurston and Smith, 1997; Verduzco et al., 2004). It is independent of inclination and provides a further means of tracking edges as well as determining depth to the top of the source structure. Unlike the Tilt angle and Theta derivatives the local wavenumber method uses second order derivatives and requires high resolution data otherwise the representation of K can be poor.

5.1.4 Residual Magnetic Imaging of Shallow Structures

The residual magnetic map over the sedimentary areas (Figure 5c) has an amplitude range within +/- 1 nT making the geological signal similar in amplitude to the noise. This makes tracking any geological signal difficult due to noise and limited resolution of the data.

Figure 5c shows the enhanced residual magnetic image over the sedimentary areas of UAE and reveals two principal structural trends. The first trend is WNW-ESE (solid white lines in Figure 5c) and tracks 2D negative anomalies while the second trend is NNE-SSW (white dashed lines in Figure 5c) and tracks 2D positive anomalies. The first trend direction could be due to the presence of shear zones identified by seismic mapping (Noufal et al., 2016) and the second trend direction could be due to faults, although they could also be due to processing artefacts since the two trend directions identified are approximately the flight line and tie line orientations of the magnetic surveys.

5.1.5 Residual Gravity Imaging of Shallow Structures

Salt basins and diapirs: Using the new gravity coverage we have expanded the study of Obaid et al. (2014), that was restricted to the offshore area covered by the Sander Geophysics gravity survey, and delineated additional salt basins (light blue dashed lines on Figure 6b) and salt diapirs (dark blue solid and dotted line closures). These are Miocene salt domes, which are sourced from a well-known and widespread evaporite sequence of Cambrian age, known as the Hormuz salt (Alsharhan and Salah, 1997). This interpretation is shown in Figure 6b where the solid dark blue lines enclose larger negative amplitude residual gravity anomalies while the dashed dark blue lines enclose smaller amplitude negative anomalies. Additional small amplitude gravity lows can be identified, but have not been highlighted. To the southeast of the Hormuz Salt Limit (thick grey dashed line close to the coast line), several

large residual gravity lows can be identified and have been identified with dark blue solid line closures. In addition, the known oil and gas fields are shown in Figure 6b.

2D linear structures: To define the shallow linear structures (faults and contacts) the THDR map has been constructed (Figure 8). The THDR is defined as

$$\text{THDR} = \sqrt{\left(\frac{\partial B}{\partial x}\right)^2 + \left(\frac{\partial B}{\partial y}\right)^2} \qquad (4)$$

where B is residual Bouguer anomaly.

The THDR maxima identify linear features such as faults and contacts while circular maxima delineate the edges of salt diapir features (Figure 8). These features can also be delineated using either Tilt angle or Theta derivatives shown in Figure 9 as images for the boxed sub area straddling the western edge of the UAE-Oman Mountains.

Topography: Since most of the structures identified in Figure 9 are shallow, we have tried to determine the influence that topography may have on the observed trends. Figure 10 has the gravity structural trends of Figure 9 superimposed on the Shuttle Radar Topographic Mission (SRTM) data. The most elevated area in the UAE is the UAE-Oman Mountains which rise over 1,000 m above sea level. However, the Musandam Peninsula has the highest elevation in the UAE with mountains of up to 2,000 m.

In the south central part of the UAE (box 1, Figure 10), the texture of the topography changes from a regional NW-SE to W-E sand dune trend to a speckled surface which continues into Saudi Arabia. The northern textural boundary is highlighted by a solid white line in Figures 8 and 10. Since this speckled topographic area closely correlates with the texture of the residual

gravity field, the likely cause is the application of an incorrect data reduction density to correct for the topographic effect of the sand dunes. This may also be the case for some of the WNW-ESE and NW-SE gravity lineaments, but not the gravity trends to the immediate west of the UAE-Oman Mountains (area delineated by box 2) shown in Figures 10b and 10c as THDR and Theta derivative maps respectively. These trends cross-cut the sand dune trends and indicate shallow sub-topographic geological sources.

Shallow structures based on the residual gravity and magnetic data: The structural maps generated from the residual magnetic and gravity maps have been combined in Figure 11 to show their correlation in the UAE-Oman Mountains area and the general lack of correlation in the sedimentary areas to the west. In the UAE-Oman Mountains, the residual gravity and magnetic maps show arcuate shallow trends that are parallel to the mountains and map the location of sub-surface thrusting as far west as the frontal thrust fault (thick black solid line in Figure 11). To the west, there is a lack of correlation between shallow structures mapped from the residual magnetic and gravity maps and the geometry features seen at shallower sedimentary levels in seismic sections. It is, therefore, inferred that the main variation in sedimentary sections occurs below the Late Jurassic Arab Formation, which is poorly imaged by seismic data. Hence, the dominant NW trending structures may express density contrast at a shallow level. However, this may also indicate structures inherited from the underlying basement. The outlines of the largest volcanic/magmatic centres, derived from the THDR of the AS of the DRTP field, are also shown in Figure 11.

5.2 Structural Lineament Trends Within the Deep Sediment Based on the Regional Gravity Data

The power spectrum analysis of the gravity data (Figure 7) indicates that in western UAE the source depths are shallower than the magnetic source depths, suggesting that potentially a major contribution of the gravity response comes from structures within the sedimentary layer and only a small contribution from the basement beneath.

A structural trend analysis was undertaken on the regional gravity data and the results are shown in Figures 12 and 13. Since the Tilt angle gradient across the contact indicates the direction of density contrast (Fairhead et al., 2011), a tick (similar to fault symbol) is used to delineate the low density side of the structural edge (similar to normal fault). Figures 12b and 12c show this, as does Figure 13a which is basically Figure 12b with only areas of positive Tilt angle ($\theta > 0.0$) shown. These positive Tilt areas could represent higher density (uplifted?) areas. The black dashed lines in Figure 13a west of the UAE-Oman Mountains do not bound or follow the Tilt angle zero contour although they are the clearest structural trends seen in other gravity-based maps (Figures 8 and 12a). This appears to be because this part of the VDR of the regional gravity is dominated by the broad high amplitude negative anomaly associated with the fore deep. Since the trends are not observed in the magnetic maps (Figures 5b and 5c) their causative structure is more than likely located in the sedimentary section as narrow 2D negative flower structures (i.e. down faulted rift-like sections of sediment) associated with the NW-SE trans-tensional strike slip faults imaged by the seismic data (see section 7.2).

The regional magnetic map (Figure 5a) has been analysed in a similar manner to the gravity data to construct the structural magnetic trend map shown in Figure 13b. The maxima of the THDR and Theta (or the zero contour of the Tilt angle) have been used to delineate the linear structural edges and the Tilt angle gradient across these edges used to define the direction of

susceptibility change. These linear structures were then superimposed on a modified Tilt angle map showing only positive Tilt angle values of the grid. Overall, the gravity and magnetic structural lineament maps (Figures 13a and 13b) show little correlation. This suggests that the gravity response due to density contrasts of the lithologies exceed those generated by the morphology and structures associated with the basement. This lack of correlation does not necessarily discount the morphology and structure of the basement based on the magnetic data (Figure 13b) as long as the sediments are non-magnetic or the top of the volcanic/magmatic sources are located close to the basement surface.

6. DEPTH TO BASEMENT

Two derivative methods have been used to estimate magnetic depth, these being the finite tilt-depth and finite local wavenumber methods. These finite depth methods have been used since most traditional methods have used infinite depth models which tend to systematically bias the 'depth to top' of the causative bodies to shallower depths. To apply the finite method, the depth of the Curie point isotherm is required, or failing this, the Moho depth is used as a proxy for this 'depth to bottom'. For the UAE the proxy used is the Crust 1.0 Moho model (Laske et al., 2013) that varies from 38.6 km in the south west to 41.6 km beneath the UAE-Oman Mountains (see inset to Figure 14a). The results of the two methods were then integrated to remove spurious depths (i.e. removal of solutions with depth differences greater than 10%). The resulting depth solutions can then be used to estimate depths of individual structural lineaments/bodies and by gridding up the depths generate a final depth map of the basement surface. Depth estimate analysis was applied to a number of versions of the regional magnetic data and included using 20 km and 10 km low-pass Butterworth (order 6) filters and a 'swing tail' filter (pages 183-184 of Fairhead, 2016). The final depth estimates

presented here are based on a 20 km low-pass Butterworth (order 6) filtered version of the DRTP magnetic grid. This filter was preferred to the other filters since it restricts the output to the long wavelength part of the spectrum controlled by deeper structures and least contaminated by shorter wavelength parts of the spectrum more strongly influenced by the volcanics and shallower structures.

6.1 Finite Tilt-Depth Method

The tilt-depth method follows Salem et al. (2014); Salem et al. (2013).

For a finite depth contact model

$$z_t = h\frac{z_b + h\tan\theta}{z_b\tan\theta - h} \qquad (5)$$

where z_t and z_b are the depths of the top and bottom of the contact model, θ is the Tilt angle at horizontal distance h from the contact where θ = 0. Since the Curie isotherm depths for the UAE are unknown, the proxy Moho depths based on Crust 1.0 model (see inset to Figure 14a) were used for depth to bottom, z_b (Salem et al., 2014).

Results of applying the finite tilt-depth method to the 20 km low-pass filtered DRTP magnetic field are shown in Figure 14a. Only those parts of the Tilt angle grid where Tilt is within θ = +/- 25° are shown and the variable separation distance of these contours, 2h, has been converted to depth z_t using equation 5. The depth z_t has then been colour coded to allow visualisation of the depth results. Depths greater than 20 km have been removed for stability of the results. Displays using θ = +/- 45° have often been used, but in this case the direct interference between the wider bands of colour made interpretation more difficult. If

an infinite tilt-depth model had been used the depths would be shallower by a mean difference of 2,050 m with std. dev. of 1,750 m.

6.2 Finite Local Wavenumber Method

For a finite depth contact model, Salem et al. (2014) showed that the maximum of the local wavenumber, K, lies directly over the contact and

$$K_{(max)} = \frac{1}{z_t} + \frac{1}{z_b} \qquad (6)$$

where z_t is depth to top and z_b is depth to bottom of the contact model.

The local wavenumber grid was calculated on the 20 km low pass filtered DRTP data set. The simple local wavenumber formulation of Verduzco et al., 2004 was used as it was seen to give more coherent results than the formulation of Phillips (2000) for this data set. Maxima were defined using the method of Blakely and Simpson (1986); limited to N=2-4 to limit the selected maxima to the more significant lineaments; again depths greater than 20 km are considered spurious and have been removed. These maximum values were then converted to depths to top, z_t, using the finite depth approach – equation 6 (Salem et al., 2014) using Crust 1.0 Moho depths for z_b 'depth to bottom'. If an infinite depth model had been used the depths would overall be shallower by a mean difference of 1,725 m with std. dev. of 1,500 m. To spatially visualise the results of the finite local wavenumber depth analysis, the depths were interpolated/extrapolated over the study area using minimum curvature (Figure 14b).

6.3 Comparison of Depths by these Methods

To compare the two sets of depth estimates, only local wavenumber depth estimates (black dots shown in Figure 14b) were used that are located within the Tilt angle contour range +/- 25°of Figure 14a. Here the Tilt angle plot has been converted to depth (colour bar in Figure 14a). The resulting cross plot of these two sets of depth estimates is shown in Figure 15. The good general agreement between the tilt-depths and local wavenumber depths for the 20 km low-pass filtered data set is clearly demonstrated in the cross-plot shown in Figure 15 where a high percentage of 'robust' solutions concentrate along the 1:1 line (i.e. similar depths are estimated from both methods). This is encouraging although not completely unexpected since the two depth estimation methods rely on similar theory, although the practical application is rather different. The mean difference between local wavenumber depths and tilt-depth estimates is 600 m (tilt-depths greater) with a std. dev. of 2,475 m. The cross-plot also shows a large number of 'poorly constrained' solutions that are causing the scatter in the cross-plot which if not removed will degrade the final depth map. One approach to cleaning up the solution space is to only accept solutions that have depths that agree to within a given depth percentage (e.g. 10%) of each other. Using this criterion, a cleaner and smoother final depth to basement map has been generated by using the local wavenumber depths within +/-10% of the corresponding tilt-depths (Figure 15) and interpolating to cover the whole area of the data (Figure 16).

7. DISCUSSION

7.1 Basement Structure and Depth Map

2D seismic profiles and exploratory well data were used to image sedimentary structures in the south-central area of the UAE to aid interpretation of the potential field data. The seismic reflections span from top Miocene evaporite to the Late Cretaceous Shu'iaba Formation (Figure 17). The Late Cretaceous formations (Nahr Umr to Simsima) thin over structural highs and disappear towards the southeast in the Mender anticline (Figure 17a). This major unconformity is coeval with the onset of obduction of the Semail Ophiolite onto the Arabian margin, and the associated flexural bulge which probably resulted in structural uplift and reactivation of basement structures (Ali and Farid, 2016).

Furthermore, the seismic reflection profiles and exploratory well data (Figures 17) suggest that the sedimentary cover of the UAE consists of lower rifted passive margin sequence (Middle Permian to Late Cretaceous), which is ca. 4 km thick, and upper foreland basins (Aruma and Pabdeh) (Ali and Watts, 2009; Boote et al., 1990). The Late Cretaceous Aruma foreland basin thickens northeastward to a maximum thickness of about 4 km along the western margin of the UAE-Oman Mountains, and that the Paleogene Pabdeh foreland in the northern UAE and west of Musandam is ca. 3 km thick (Ali et al., 2013; Ricateau and Riche, 1980). This suggests that the basement is considered to lie at least 3 km to 4 km beneath the lowest reflectors that are imaged in Figure 17. Although seismic data do not image the basement directly, they indicate that the basement must be below 9 km.

Moreover, the final basement depth map of the UAE (Figure 16) shows the UAE-Oman Mountain belt has depths to magnetic sources of less than 1000 m. Rather than crystalline magnetic basement, these shallow depth results are more than likely due to the presence of near surface volcanic related features. This is because the primary source of the magnetic signature is from the thick ophiolite rocks which are either exposed or close to the surface.

The magnetic basement is deepest in the eastern foreland basin, immediately west of the UAE-Oman ophiolite. This is consistent with the backstripped, flexure and finite rifting modelling derived basement depths (Ali and Watts, 2009).

The magnetic basement shows the Mender and Lekhwair oilfields in the southeast of the UAE are characterised by relatively deep basement (>10 km) although the seismic profiles over the area (Figure 17a), indicate sedimentary and basement uplift. In this area, the seismic and well data suggest absence of Middle and Late Cretaceous sediments, which was caused by a major uplift and erosional event that occurred during the obduction of the Semail Ophiolite in the Late Cretaceous (Ali and Farid, 2016). Furthermore, the regional Bouguer gravity map shows a positive anomaly over the area (Figure 6a), which may indicate a basement uplift. This discrepancy can be explained by assuming that the magnetic basement low is because the magnetic signature comes from structures deep within the basement, whereas the high gravity anomaly is caused by high density contrast between the basement and sedimentary cover.

To the west of the foreland basin, the basement surface takes on a somewhat simple set of N-S to NNE-SSW trending basement ridges reaching to less than 5 km depth in places and flanked by structural edges interpreted as border faults. The intervening troughs exceed 15 km depth in places. These N-S to NNE-SSW trending ridges appear to be disrupted by a WNW-ESE zone of dextral displacement as shown in the simple tectonic map (Figure 18). Superimposed on the simple tectonic map are the main volcanic/magmatic centres. The majority of the oilfields appear to be restricted to the central foreland of the UAE. This could indicate that the oil productive basins have been controlled by the location of the basement ridges. Since the deeper parts of sedimentary sections and basement have not been imaged

seismically, the interpretation of the gravity and magnetic data in terms of faulting, basement ridges and troughs is highly speculative but it at least provides a model that can be tested by future seismic studies. The troughs and anticlinal ridges could have been basin rifting faults that have been reactivated during the Late Cretaceous due to the emplacement of the UAE-Oman Mountains. Therefore, the development of onshore traps, such as the Shah, Asab, Sahil and Bu Hasa anticlines have been strongly influenced by the structural trends of basement highs. Transpression along WNW-ESE trending wrench faults may also form positive flower structures that can develop traps. In the offshore areas, salt diapirs controlled the development of salt-cored anticlines and salt flank structures, such as the Gasha-Butini and Hail fields.

7.2 Structural Lineaments and Seismic Equivalents

In the UAE, no wells penetrate basement and available seismic data do not clearly image structures below the Permian Khuf Formation (ca 3.5 km to 5.4 km). Thus, gravity and magnetic data can greatly contribute to our knowledge and understanding of the morphology of the basement and basinal structures. Both the residual (Figure 11) and regional (Figures 12 and 13) gravity and magnetic data clearly indicate three well-defined lineaments (WNW-ESE to NW-SE, N-S to NNE-SSW and NE-SW) in the UAE. These trends can be clearly identified in the curvature map derived from 2D and 3D seismic data (Figure 19).

7.2.1 WNW-ESE to NW-SE Trends

These trends are best seen in both the residual gravity and magnetic data (Figure 11) within the sedimentary sequence using a power spectrum pseudo depth slice of ~0.9 km +/- 0.2 km for all of the UAE west of the UAE-Oman Mountains. Ali et al. (2014) have named these

trends the Abu Dhabi Lineaments. These faults are clearly seen in the curvature map of the top Shu'iaba Formation at ca. 1.4 km to 3.3 km depth (Figure 19), and are interpreted as predominately strike-slip faults that extend across the full width of the UAE (Figure 19). These faults have little to no vertical displacement of strata or rock units on either side (Noufal et al., 2016) and appear to form shallow saddle regions that separate narrower sub-basins in the central UAE, from a broader sub-basin development in the north and the south. They are made up of numerous individual faults with fault bends, offsets, terminations and branching that can lead to local areas of uplift (transpression) and subsidence (transtension). These faults cut and sinistrally offset or deform the N-S trending and NE-SW trending faults (Figure 19) and thus appear younger in age which could represent the reactivation of older structures. These lineaments have a similar trend to the Proterozoic sinistral shear Najd Fault System that cut through Saudi Arabia.,(Al-Husseini, 2000). However, the NW-SE trend has also a similar trend to the shelf-slope break associated with the younger Tethyan rifted margin hinge zone (Ali et al., 2014). In the northern eastern part of UAE, west of the UAE-Oman Mountains, the NW-SE (N45°W) trending faults are dominant features in both the seismic and gravity but not in the magnetic map.

7.2.2 N-S to NNE-SSW Trends

These trends dominate both the residual and regional gravity and magnetic maps as well as the seismic maps of western UAE. Several onshore giant oilfields in Abu Dhabi (e.g. Bu Hasa) lie along these trends. These trends probably reflect deep basement structures such as the original Neoproterozoic tectonic elements of the Arabian Plate which have been periodically reactivated (Edgell, 1990) resulting in them being seen in the residual gravity and magnetic data and shallow seismic data.

7.2.3 NE-SW Trends

This trend is represented by major discontinuities which extend across the south-central and northern-western parts of the UAE. Locally, these lineaments appear to mark a change in intra-basin gravity relief, thus are probably structural reliefs. Structures of the giant onshore oilfields Shah, Asab and Sahil (Figure 1) are located along one such NE-SW lineament in south central UAE.

The trend may reflect a NE trending Neoproterozoic compressional event in the Arabian Plate that involved shear zones and basement thrust faults (Ali et al., 2014). Furthermore, the NE-SW trend corresponds to the main trend of the Hormuz Salt basin in the Arabian Gulf and the Ara Salt basin in central Oman, and appears to control the distribution of infra-Cambrian salt basins of the Arabian Gulf and Oman (Al-Husseini, 2000; Loosveld et al., 1996).

8. CONCLUSIONS

The following major conclusions can be drawn from this study:

- The countrywide analysis of the gravity and aeromagnetic data west of the UAE-Oman Mountains has resulted in structural trend maps of both the shallow (~1 km) and deep (5 km to 15 km) basinal sections.
- The resolution of the structures associated with the shallowest density and susceptibility interface is limited due to noise in the data due to the age of the data (acquisition and processing) and the digital cell size of the grid data provided. However, the gravity residual map does delineate the salt diapirs well and a series of

2D linear features trending NW-SE across the UAE. This NW-SE trend is only poorly seen in the residual magnetic data.

- By assuming the sediments are non-magnetic and the basement magnetic we have used the regional magnetic data to map the depth to basement. The map reveals a set of NNE-SSW trending ridges ~5 km depth with dextral offset towards their southern end and separated from each other by deep basinal areas.
- The regional gravity structural interpretation does not correlate well with the magnetic structural interpretation. This lack of correlation can be explained by gravity response associated with the lateral lithological density variation within the sedimentary section being much larger than the gravity response resulting from the morphology of the basement surface. The argument used above is that the basement has a constant density. Although this may be a reasonable assumption, in the southeast corner of UAE the Mender anticline has a known domal structure associated with obduction of the Semail Ophiolite and has resulted in the erosion or non-deposition of Middle-Late Cretaceous sediments. Here one would expect from the seismic and gravity data that the basement surface be domally uplifted, whereas the magnetic basement depths are large suggesting possibly non-magnetic basement is present such as a granite.
- In determining the depth to basement, a technique was implemented to allow the depth results from finite tilt-depth and finite local wavenumber methods to be compared so that only solutions with depths agreeing to within 10% of each other were accepted. This provided a cleaner set of depth solutions that could be mapped into a final depth grid. This mapping method has its limitations as magnetic depth solutions tend to image shallow structure and basement uplifts/highs rather than the deepest parts of the sedimentary basins/troughs. These uplifted structures are

important for hydrocarbon accumulation although depths in the deepest parts of the basin are also important for basin modelling.

- Using this final depth grid and structural lineament trends a simple shear tectonic model at depth has been proposed that links and offsets a series of N-S basement highs and volcanic/magmatic centres. Reactivation of deep shear zones could explain the numerous NW-SE trending faults seen in the residual magnetic and gravity maps as well as seismically derived curvature map. Additionally, the basement faults bounding the N-S trending basement highs could explain the increased mobilization of the salt and associated hydrocarbon accumulations.

9. ACKNOWLEDGEMENTS

We are grateful to the Petroleum Institute for sponsoring this project. We wish to thank ADNOC for permission to publish the data used in this study. We thank Mark Pilkington and an anonymous reviewer for their helpful comments.

10. REFERENCES

Al-Husseini, M.I., 2000. Origin of the Arabian Plate structures; Amar collision and Najd Rift. GeoArabia (Manama) 5, 527-542.

Al-Husseini, M.I., Matthews, R.K., 2010. Calibrating mid-Permian to Early Triassic Khuff sequences with orbital clocks. GeoArabia (Manama) 15, 171-206.

Ali, M.Y., Farid, A., 2016. CRETACEOUS – NEOGENE STRUCTURAL EVOLUTION OF SE ABU DHABI, UNITED ARAB EMIRATES. Journal of Petroleum Geology 39, 221-245.

Ali, M.Y., Watts, A.B., 2009. Subsidence history, gravity anomalies and flexure of the United Arab Emirates (UAE) foreland basin. GeoArabia 14, 17-44.

Ali, M.Y., Watts, A.B., Farid, A., 2014. Gravity anomalies of the United Arab Emirates: Implications for basement structures and infra-Cambrian salt distribution. GeoArabia 19, 85-112.

Ali, M.Y., Watts, A.B., Searle, M.P., 2013. Seismic stratigraphy and subsidence history of the United Arab Emirates (UAE) rifted margin and overlying foreland basins, in: Hosani, K.A., Roure, F., Ellison, R., Lokier, S. (Eds.), " Lithosphere Dynamics and Sedimentary Basins: The Arabian Plate and Analogues. Springer-Verlag Berlin Heidelberg, pp. 127-143.

Alsharhan, A.S., Salah, M.G., 1997. Tectonic implications of diapirism on hydrocarbon accumulation in the United Arab Emirates. B Can Petrol Geol 45, 279-296.

Arkani-Hamed, J., 2007. Differential reduction to the pole: Revisited. GEOPHYSICS 72, L13-L20.

Benson, A.K., Floyd, A.R., 2000. Application of gravity and magnetic methods to assess geological hazards and natural resource potential in the Mosida Hills, Utah County, Utah. Geophysics 65, 1514-1526.

Blakely, R.J., Simpson, R.W., 1986. Approximating edges of source bodies from magnetic or gravity anomalies. Geophysics 51, 1494-1498.

Blendinger, W., Van Vliet, A., Clarke, M.W.H., 1990. Updoming, rifting and continental margin development during the late Palaeozoic in northern Oman. Geological Society Special Publications 49, 27-37.

Bloch, G., 2000. Shah field Simsima 3D seismic re-interpretation report, unpublished report, pp. 1-38.

Boote, D.R.D., Mou, D., Waite, R.I., Robertson, A.H.F., Searle, M.P., Ries, A.C., 1990. Structural evolution of the Suneinah Foreland, central Oman Mountains. Geological Society Special Publications 49, 397-418.

Edgell, H.S., 1990. Basement tectonics of Saudi Arabia as related to oil field structures. Proceedings of the International Conference on Basement Tectonics 9, 169-193.

Fairhead, J.D., 2016. Advances in Gravity and Magnetic Processing and Interpretation. EAGE Publications bv.

Fairhead, J.D., Salem, A., Cascone, L., Hammill, M., Masterton, S., Samson, E., 2011. New developments of the magnetic tilt-depth method to improve structural mapping of sedimentary basins. Geophysical Prospecting 59, 1072-1086.

Glennie, K.W., Boeuf, M.G., Clarke, M.W.H., Moody-Stuart, M., Pilaar, W.F.H., Reinhardt, B.M., 1974. The Geology of the Oman Mountains. Verhandelingen van het Koninklijk Nederlands Geologisch Mijnbouwkundig Genootschap 31.

Hinze, W.J., Frese, R.R.B.v., Saad, A.H., 2013. Gravity and Magnetic Exploration: Principles, Practices, and Applications. Cambridge University Press, New York.

Jallouli, C., Mickus, K.L., Moncef Turki, M., 2002. Gravity constraints on the structure of the northern margin of Tunisia: implications on the nature of the northern African Plate boundary. Geophysical Journal International 151, 117-131.

Karner, G.D., Watts, A.B., 1983. Gravity anomalies and flexure of the lithosphere at mountain ranges. Journal of Geophysical Research 88, 10449-10477.

Khattab, M.M., 1995. Interpretation of Magnetic and Gravity Surveys in the Southern Arabian Gulf, the Strait of Hormuz, and the Northwesternmost Gulf of Oman - Implications of Pre-Permian Basement Tectonics. Mar Geol 123, 105-116.

King, M.S., Barr, S.M., 2004. Magnetic and gravity models across terrane boundaries in southern New Brunswick, Canada. Canadian Journal of Earth Sciences 41, 1027-1047.

Konert, G., Afifi, A.M., Al-Hajri, S.i.A., Droste, H.J., 2001. Paleozoic stratigraphy and hydrocarbon habitat of the Arabian Plate. GeoArabia (Manama) 6, 407-442.

Laske, G., Masters, G., Ma, Z., Pasyanos, M., 2013. Update on CRUST1.0 - A 1-degree Global Model of Earth's Crust, EGU2013. EGU, p. 2658.

Loosveld, R.J.H., Bell, A., Terken, J.J.M., 1996. The tectonic evolution of interior Oman. GeoArabia (Manama) 1, 28-51.

Manghnani, M.H., Coleman, R.G., 1981. Gravity profiles across the Samail ophiolite, Oman. Journal of Geophysical Research 86, 2509-2525.

Nolan, S.C., Skelton, P.W., Clissold, B.P., Smewing, J.D., 1990. Maastrichtian to early Tertiary stratigraphy and palaeogeography of the central and northern Oman Mountains. Geological Society Special Publications 49, 495-519.

Noufal, A., Obaid, K., Ali, M.Y., 2016. Tectonic Map of Abu Dhabi, UAE. Society of Petroleum Engineers.

Obaid, K.A., Neves, F., Mahgoub, M.A.E.G., Taher, A., Noufal, A., Matarid, T.M., Inoue, H., 2014. Enhanced Interpretation Of Salt-Related Structures In Abu Dhabi Using Improved Seismic Data Processing And Interpretation Techniques. Society of Petroleum Engineers.

Patton, T.L., O'Connor, S.J., 1988. Cretaceous flexural history of northern Oman Mountain foredeep, United Arab Emirates. AAPG Bulletin 72, 797-809.

Phillips, J.D., 2000. Locating magnetic contacts: a comparison of the horizontal gradient, analytic signal, and local wavenumber methods, SEG 2000 Expanded Abstracts. SEG, pp. 402-405.

Phillips, J.D., 2001. Designing matched bandpass and azimuthal filters for the separation of potential field anomalies by source region and source type, 15th Geophysical Conference and Exhibition, Australian Society of Exploration Geophysicists. ASEG, Brisbane.

Ravaut, P., Bayer, R., Hassani, R., Rousset, D., AlYahyaey, A., 1997. Structure and evolution of the northern Oman margin: gravity and seismic constraints over the Zagros-Makran-Oman collision zone. Tectonophysics 279, 253-&.

Ricateau, R., Riche, P.H., 1980. Geology of the Musandam Peninsula (Sultanate of Oman) and its surroundings. Journal of Petroleum Geology 3, 139-152.

Robertson, A.H.F., Searle, M.P., 1990. The northern Oman Tethyan continental margin; stratigraphy, structure, concepts and controversies. Geological Society Special Publications 49, 3-25.

Ruban, D.A., Al-Husseini, M.I., Iwasaki, Y., 2007. Review of Middle East Paleozoic plate tectonics. Geoarabia 12, 35-55.

Salem, A., Ali, M.Y., 2016. Mapping basement structures in the northwestern offshore of Abu Dhabi from high-resolution aeromagnetic data. Geophysical Prospecting 64, 726-740.

Salem, A., Blakely, R., Green, C., Fairhead, D., Ravat, D., 2014. Estimation of depth to top of magnetic sources using the local-wavenumber approach in an area of shallow Moho and Curie depth — The Red Sea. Interpretation 2, SJ1-SJ8.

Salem, A., Campbell, S., Moorhead, L., Fairhead, J.D., 2013. An Enhanced Tilt Depth Method for Interpreting Magnetic Data over Vertical Contacts of Finite Extent, 75th EAGE Conference & Exhibition EAGE, pp. Exhibition Extended Abstracts Tu P03 06, doi:10.3997/2214-4609.20130595.

Salem, A., Williams, S., Fairhead, D., Smith, R., Ravat, D., 2007. Interpretation of magnetic data using tilt-angle derivatives. Geophysics 73, L1-L10.

Searle, M.P., 2007. Structural geometry, style and timing of deformation in the Hawasina window, Al Jabal al Akhdar and Saih Hatat culminations, Oman mountains. GeoArabia 12, 99-130.

Searle, M.P., Warren, C.J., Waters, D.J., Parrish, R.R., 2004. Structural evolution, metamorphism and restoration of the Arabian continental margin, Saih Hatat region, Oman Mountains. Journal of Structural Geology 26, 451-473.

Sharland, P.R., Archer, R., Casey, D.M., Davies, R.B., Hall, S.H., Heward, A.P., Horbury, A.D., Simmons, M.D., 2001. Arabian plate sequence stratigraphy. Gulf Petro-Link, Manama.

Shelton, A.W., 1990. The interpretation of gravity data in Oma: constraints on the ophiolite emplacement mechanism, in: Robertson, A.H.F., Searle, M.P. (Eds.), The Geology and Tectonics of the Oman Region. Geological Society Special Publication, London, pp. 459-471.

Spector, A., Grant, F.S., 1970. Statistical models for interpreting aeromagnetic data. Geophysics 35, 293-302.

Stewart, J., Watts, A.B., 1997. Gravity anomalies and spatial variations of flexural rigidity at mountain ranges. Journal of Geophysical Research: Solid Earth 102, 5327-5352.

Thurston, J.B., Smith, R.S., 1997. Automatic conversion of magnetic data to depth, dip, and susceptibility contrast using the SPI (TM) method. GEOPHYSICS 62, 807-813.

Treitel, S., Clement, W.G., Kaul, R.K., 1971. The Spectral Determination of Depths to Buried Magnetic Basement Rocks. Geophysical Journal of the Royal Astronomical Society 24, 415-428.

Verduzco, B., Fairhead, J.D., Green, C.M., MacKenzie, C., 2004. New insights into magnetic derivatives for structural mapping. The Leading Edge 23, 116-119.

Warren, C.J., Parrish, R.R., Waters, D.J., Searle, M.P., 2005. Dating the geologic history of Oman's Semail Ophiolite; insights from U/Pb geochronology. Contributions to Mineralogy and Petrology 150, 403-422.

Warsi, W.E.K., 1990. Gravity field of Kuwait and its relevance to major geological structures. AAPG Bulletin (American Association of Petroleum Geologists); (United States), Medium: X; Size: Pages: 1610-1622.

White, D.J., Thomas, M.D., Jones, A.G., Hope, J., Németh, B., Hajnal, Z., 2005. Geophysical transect across a Paleoproterozoic continent–continent collision zone: The Trans-Hudson Orogen. Canadian Journal of Earth Sciences 42, 385-402.

Ziegler, M.A., 2001. Late Permian to Holocene paleofacies evolution of the Arabian Plate and its hydrocarbon occurrences. GeoArabia (Manama) 6, 445-504.

Figure Captions

Figure 1. Surface geology map of the United Arab Emirates (UAE) and northern Oman (simplified from Searle (2007)). Green-coloured ovals show the locations of oilfields with major structural trends at Early Cretaceous level. Blue lines and black circles represent seismic profiles and exploration wells, respectively that are shown in Figures 17a and 17b. GO denotes the Gulf of Oman.

Figure 2. Gravity station and aeromagnetic coverages. The orange area shows aeromagnetic coverage in the UAE. Blue filled polygon shows the Sander Geophysics survey.

Figure 3. Aeromagnetic maps of the UAE. a) Total Magnetic Intensity (TMI) and b) Differential Reduced To Pole (DRTP) map showing the four power spectrum window locations for magnetic (Figure 4) and gravity (Figure 7) analysis. Black, red and blue dots show centre locations of all power spectrum windows used in the analysis. The 14 black dots are locations where the gravity depth estimate for the deeper segment is less than the magnetic equivalent and the 6 blue dots where the gravity depth estimate is greater than the magnetic equivalent. White dots are principal towns/cities.

Figure 4. Examples of four magnetic power spectrum plots with window sizes 100 km x 100 km, as shown in Figure 3b. a) Window 1 centred at 53°E, 25°N, b) Window 2 centred at 53°E, 23.5°N, c) Window 3 centred at 56.1°E, 25.4°N, d) Window 4 centred at 55.4°E, 24.1°N. An intermediate segment highlighted by red dashed line in Window 1 suggests the presence of an additional layer at about 4 km to 5 km depth. Evidence for this segment is also seen in Windows 2 and 4. Window 3 is over the UAE-Oman Mountains and shows

significant change in form of the power spectrum. The x axis of the power spectrum plots has two scales a non-linear wavelength, λ scale, extending from the Nyquist wavelength (2 x grid cell size) to infinity and the linear wavenumber K scale extending from zero to π (where K = Nyquist wavelength $* \pi/\lambda$). Depths stated are below survey height datum of 518 m (above mean sea level).

Figure 5. a) Regional and b) Residual magnetic DRTP maps using an order 6 Butterworth filter centred on 10 km. The thick solid black line delineates the western most structural boundary seen in the magnetic data. The red box is the region shown in c) which is the residual magnetic DRTP anomaly map restricted to the area west of the UAE-Oman Mountains. Due to small dynamic amplitude range of the residual anomaly over most of UAE, the area west of 55.4°E has been colour equalised separately to enhance subtle anomaly trends shown as solid white lines for NW-SE and dashed white lines for N-S trends.

Figure 6. a) Regional and (b) residual Bouguer gravity maps using a Butterworth filter centred on 25 km showing shallow structural trends (thin dashed black lines) as well as locations of potential salt basins and diapirs. Also overlain (in pink outlines) are oil and gas fields after Ali et al. (2014). The Hormuz Salt Limit is delineated by thick grey dashed line located close to the coastline.

Figure 7. Gravity power spectrum plots for the four window locations shown in Figure 3b. Like the magnetic spectra (Figure 4) they generally show a clear separation between shallow and deep structures.

Figure 8. The total horizontal derivative (THDR) of the residual gravity map for areas west of the UAE-Oman Mountains with 100% colour equalisation. Polygonal areas of poor gravity coverage are shown and the arcuate zone (outlined by solid white line) close to and along the southern border of the UAE shows a change in the gravity anomaly character/texture.

Figure 9. Structural trends observed in the residual gravity data (Figures 6b and 8). Linear trends show up well within the UAE-Oman Mountains - grey shaded area with its western extent delineated by the thick black line. Elsewhere in the sedimentary areas the linear trends are poorly defined except for the circular salt diapirs defined by the thick blue lines. The red inset boxes, shown to the right, provide examples of the Tilt angle and Theta derivative maps used in addition to THDR (Figure 8) to define the structural trends. The black and white arrows highlight NW-SE structural trends and frontal thrust fault.

Figure 10. a) The onshore gravity structural trends of Figure 9 superimposed on the Shuttle Radar Topography Mission (SRTM) topographic map of the UAE. The change in surface topographic texture outlined by the white line in southern central UAE has been enhanced within the inset box area (box 1). The box area (box 2) over the UAE-Oman Mountains is shown in more detail in Figures 10b and c. b) Gravity derived structural trends based on the THDR of residual Bouguer anomaly and location of outer thrust zone as thick black line. c) Magnetic derived structural trends (white denotes maxima or edges) based on the Theta derivative and location of outer thrust zone as thick black line. White dots are principal towns/cities.

Figure 11. Compilation of structural trends derived from the residual magnetic and gravity maps (Figures 5b, 5c and 9). The outlines of the volcanic/magnetic centres were derived from the THDR of the AS of the DRTP field.

Figure 12. Mapping the intermediate depth structures based on the regional gravity map that images structures in the deep sedimentary section. a) THDR of the regional Bouguer anomaly, b) Tilt angle of the regional Bouguer gravity and c) Theta of the regional Bouguer anomaly. Solid black lines represent edges and tick marks indicate lower density side of the edge structures**.**

Figure 13. a) Similar to Figure 12b showing the intermediate depth structures based on the regional gravity map that images structural trends in both the deep sedimentary section and basement but now superimposed only on the positive component of the Tilt angle. b) Basement structure trends (faults and contacts) based on the interpretation of the regional magnetic anomaly map superimposed on the positive Tilt angle of the magnetic anomaly (i.e. $\theta > 0.0$). Tick marks indicate lower susceptibility side of the edge structures**.**

Figure 14. a) Finite tilt-depth plot of the regional magnetic field derived from 20 km low pass filtered magnetic grid and Crust 1.0 Moho model (inset) as a proxy for the depth of the Curie isotherm. The colour depth legend is defined by the width of the Tilt angle contours in the range +/- 25°. b) Finite local wavenumber method depth estimates after Phillips (2000) expanded by minimum curvature gridding to cover the whole of the study area. Black dots are the maxima of the local wavenumber grid and represent the points at which the depth was initially estimated.

Figure 15. Cross-plot of finite tilt-depth against gridded finite local wavenumber depth estimates, both based on the 20 km low pass filtered DRTP data set. Colours represent density of points. Solutions that lie within the depth range of +/- 10% of each other are used to generate the final depth map (Figure 16).

Figure 16. Basement structure and depth map based on finite local wavenumber depth estimates which are within 10% tolerance of the finite tilt depth estimate at the same point. Overlay shows basement structural elements shown in Figure 13b.

Figure 17. a) NW-SE oriented composite seismic profiles over the Shah, Zararrah, Qusahwira and Mender anticlines. See Figure 1 for locations. Thick black line represents top of Shu'iaba Formation. b) SW-NE oriented composite seismic profiles over the south eastern region of UAE. See Figure 1 for locations. Thick black line represents top of Shu'iaba Formation.

Figure 18. Schematic tectonic map of the UAE. The map highlights basement ridges in bold red lines and positions a WNW-ESE dextral shear structure between the offsets of similar direction as seen in the residual magnetic data but whose location is midway between the two main shears seen in the south-east of the UAE. Superimposed on the simple tectonic map are the main volcanic/magmatic centres.

Figure 19 Curvature map of top Shu'iaba Formation (see Figure 17 for approximate depth) in Abu Dhabi emirate showing the main fault system in the area. The map was generated from large 3D and 2D seismic data sets in Abu Dhabi. The map shows major lineaments in the sedimentary cover. Green arrows indicate the N-S and NNW-SSE trending faults; blue arrows show NW-SE trending faults, and red arrows depict the NE-SW trending faults.

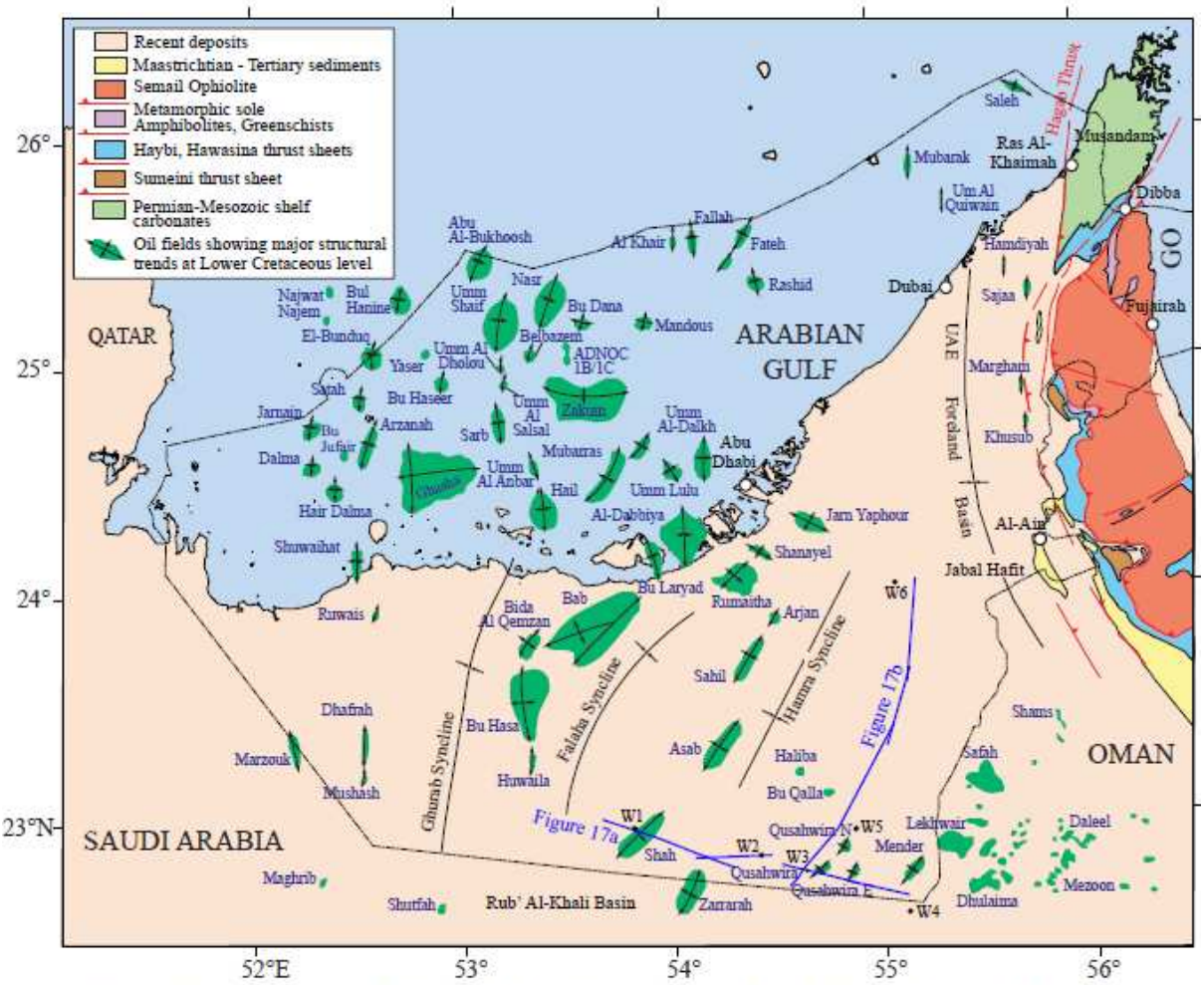

Figure 1. Surface geology map of the United Arab Emirates (UAE) and northern Oman (simplified from Searle (2007)). Green-coloured ovals show the locations of oilfields with major structural trends at Early Cretaceous level. Blue lines and black circles represent seismic profiles and exploration wells, respectively that are shown in Figures 17a and 17b. GO denotes the Gulf of Oma

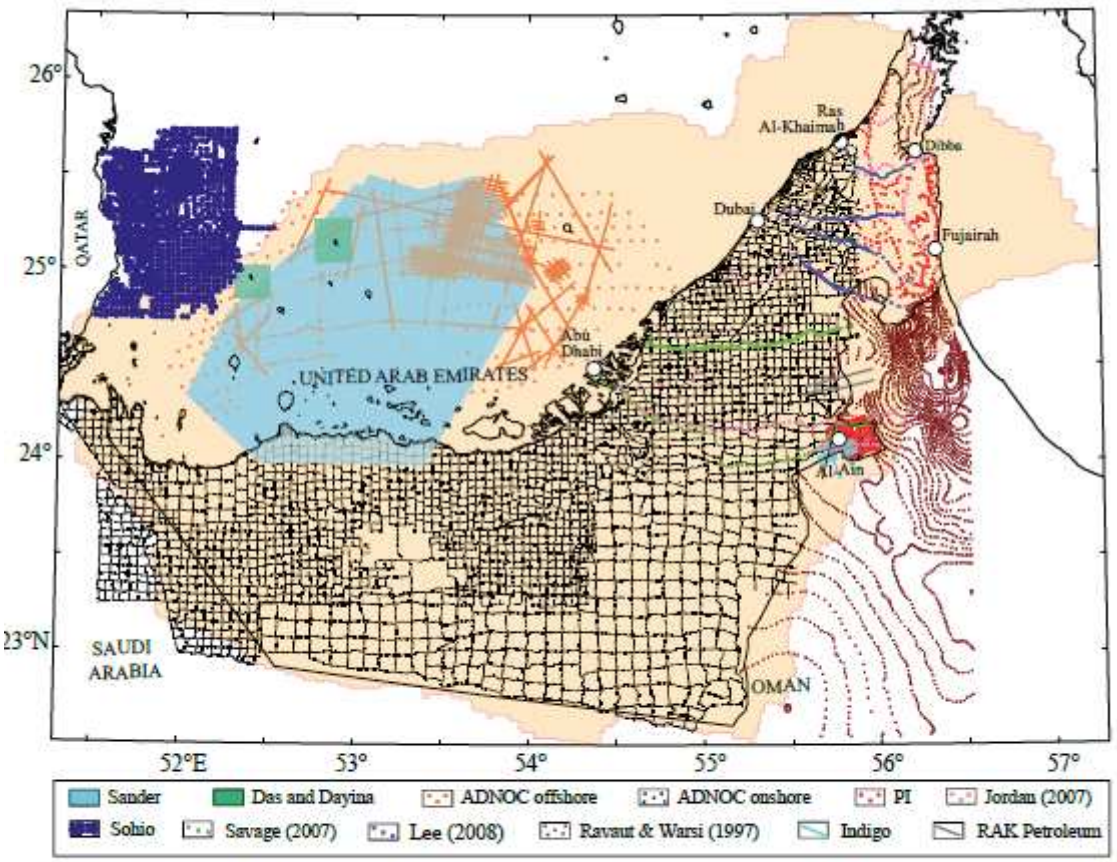

Figure 2. Gravity station and aeromagnetic coverages. The orange area shows aeromagnetic coverage in the UAE. Blue filled polygon shows the Sander Geophysics survey.

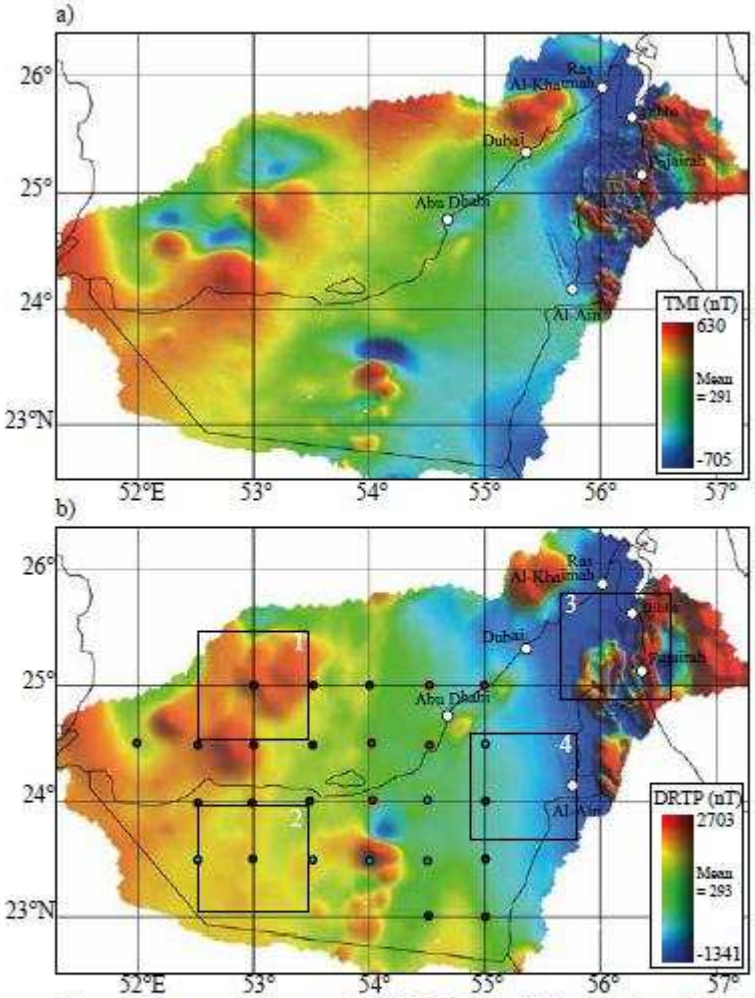

Figure 3. Aeromagnetic maps of the UAE. a) Total Magnetic Intensity (TMI) and b) Differential Reduced To Pole (DRTP) map showing the four power spectrum window locations for magnetic (Figure 4) and gravity (Figure 7) analysis. Black, red and blue dots show centre locations of all power spectrum windows used in the analysis. The 14 black dots are locations where the gravity depth estimate for the deeper segment is less than the magnetic equivalent and the 6 blue dots where the gravity depth estimate is greater than the magnetic equivalent. White dots are principal towns/cities.

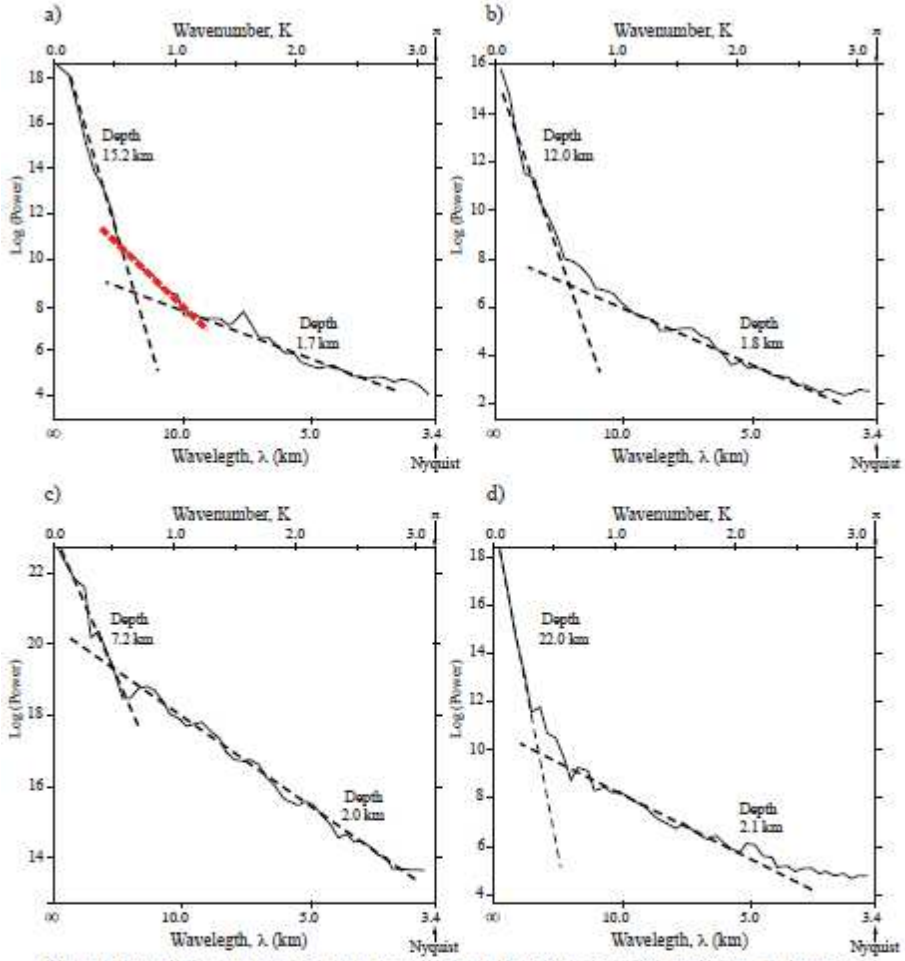

Figure 4. Examples of four magnetic power spectrum plots with window sizes 100 km x 100 km, as shown in Figure 3b. a) Window 1 centred at 53°E, 25°N, b) Window 2 centred at 53°E, 23.5°N, c) Window 3 centred at 56.1°E, 25.4°N, d) Window 4 centred at 55.4°E, 24.1°N. An intermediate segment highlighted by red dashed line in Window 1 suggests the presence of an additional layer at about 4 km to 5 km depth. Evidence for this segment is also seen in Windows 2 and 4. Window 3 is over the UAE-Oman Mountains and shows significant change in form of the power spectrum. The x axis of the power spectrum plots has two scales a non-linear wavelength, λ scale, extending from the Nyquist wavelength (2 x grid cell size) to infinity and the linear wavenumber K scale extending from zero to π (where K = Nyquist wavelength *π/λ). Depths stated are below survey height datum of 518 m (above mean sea level).

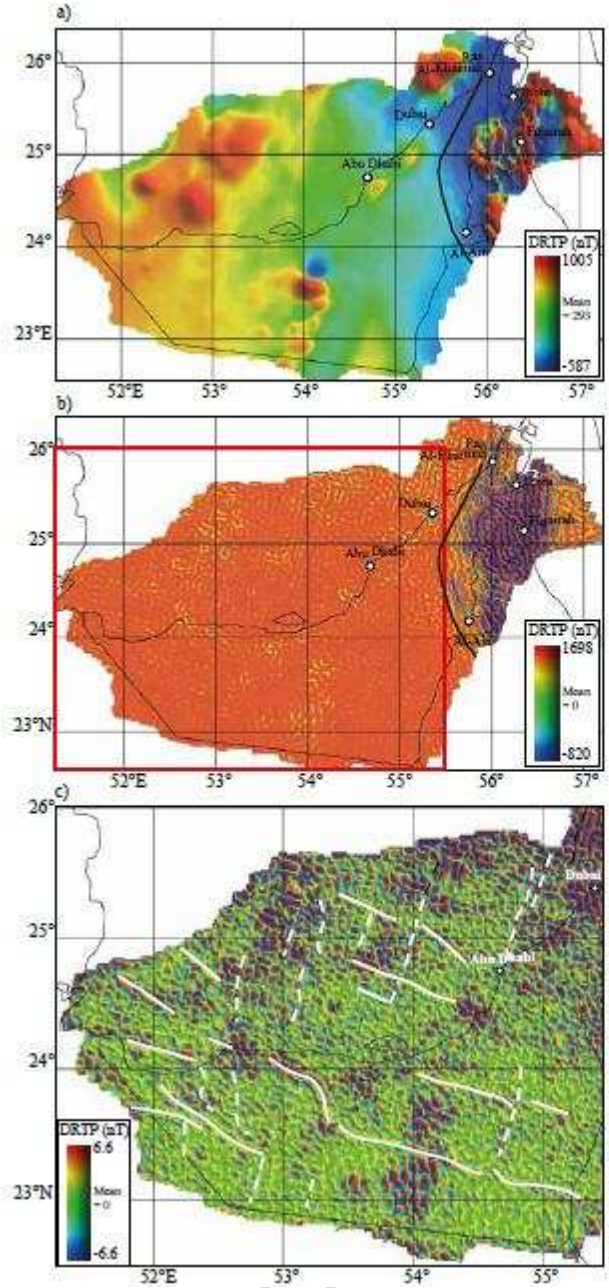

Figure 5. a) Regional and b) Residual magnetic DRTP maps using an order 6 Butterworth filter centred on 10 km. The thick solid black line delineates the western most structural boundary seen in the magnetic data. The red box is the region shown in c) which is the residual magnetic DRTP anomaly map restricted to the area west of the UAE-Oman Mountains. Due to small dynamic amplitude range of the residual anomaly over most of UAE, the area west of 55.4°E has been colour equalised separately to enhance subtle anomaly trends shown as solid white lines for NW-SE and dashed white lines for N-S trends.

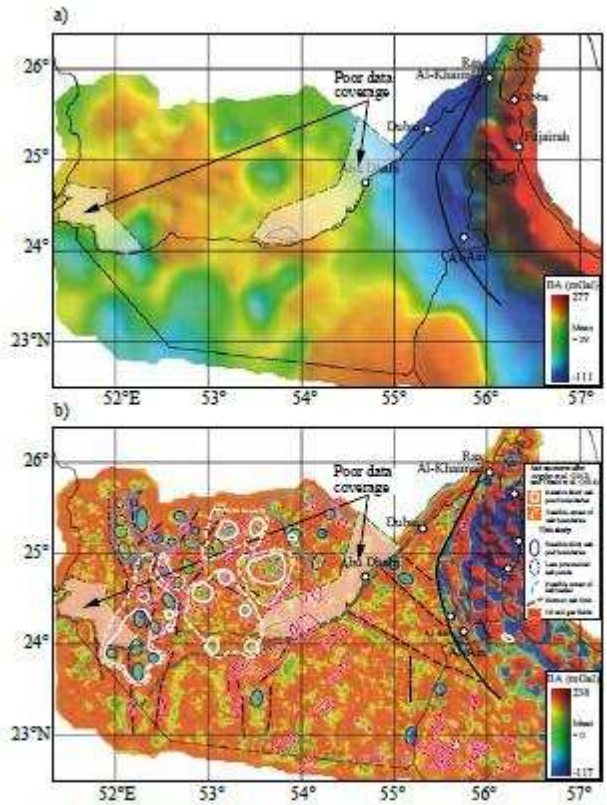

Figure 6. a) Regional and (b) residual Bouguer gravity maps using a Butterworth filter centred on 25 km showing shallow structural trends (thin dashed black lines) as well as locations of potential salt basins and diapirs. Also overlain (in pink outlines) are oil and gas fields after Ali et al. (2014). The Hormuz Salt Limit is delineated by thick grey dashed line located close to the coastline.

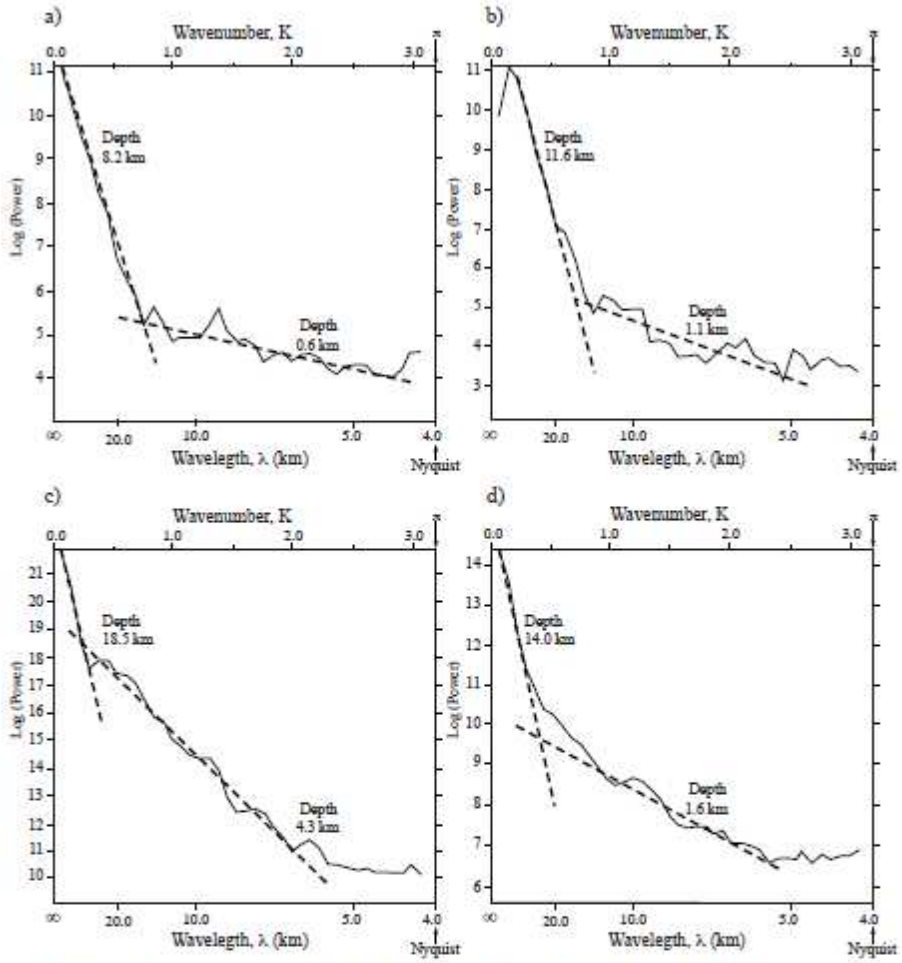

Figure 7. Gravity power spectrum plots for the four window locations shown in Figure 3b. Like the magnetic spectra (Figure 4) they generally show a clear separation between shallow and deep structures.

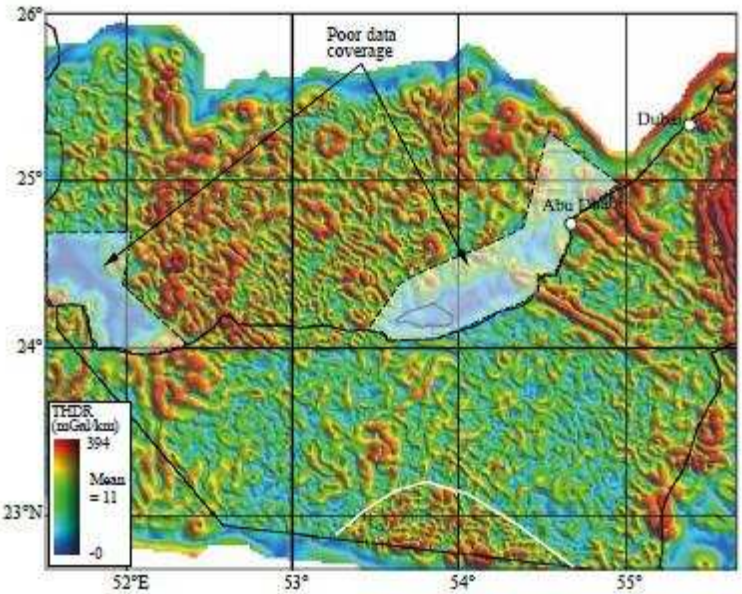

Figure 8. The total horizontal derivative (THDR) of the residual gravity map for areas west of the UAE-Oman Mountains with 100% colour equalisation. Polygonal areas of poor gravity coverage are shown and the arcuate zone (outlined by solid white line) close to and along the southern border of the UAE shows a change in the gravity anomaly character/texture.

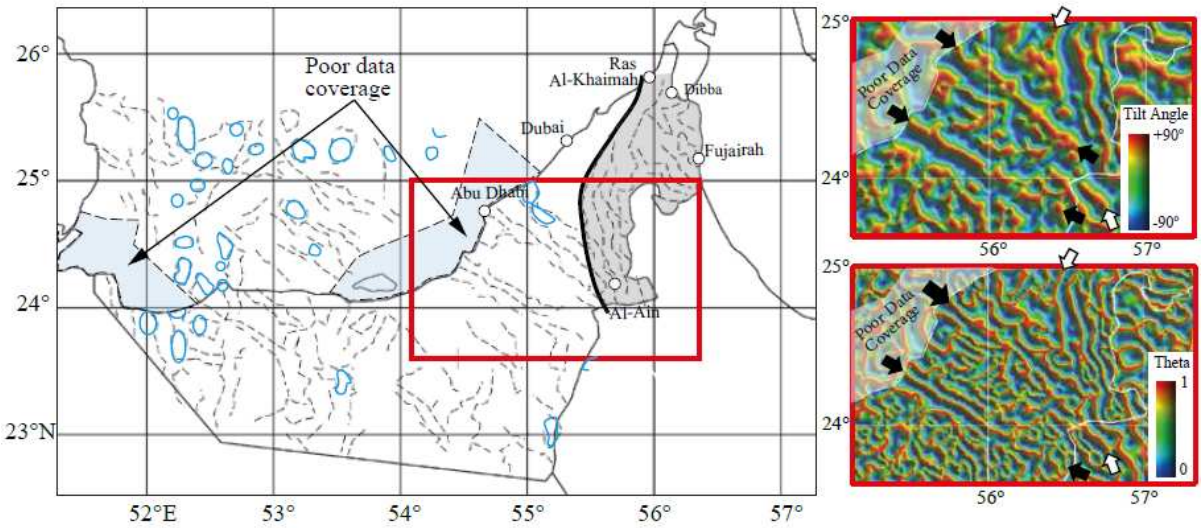

Figure 9. Structural trends observed in the residual gravity data (Figures 6b and 8). Linear trends show up well within the UAE-Oman Mountains - grey shaded area with its western extent delineated by the thick black line. Elsewhere in the sedimentary areas the linear trends are poorly defined except for the circular salt diapirs defined by the thick blue lines. The red inset boxes, shown to the right, provide examples of the Tilt angle and Theta derivative maps used in addition to THDR (Figure 8) to define the structural trends. The black and white arrows highlight NW-SE structural trends and frontal thrust fault.

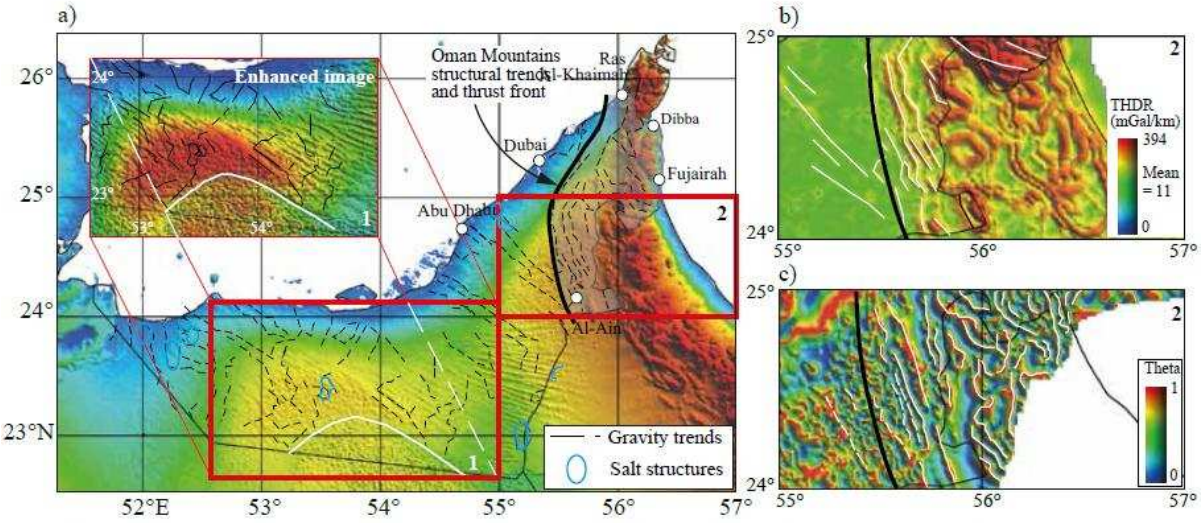

Figure 10. a) The onshore gravity structural trends of Figure 9 superimposed on the Shuttle Radar Topography Mission (SRTM) topographic map of the UAE. The change in surface topographic texture outlined by the white line in southern central UAE has been enhanced within the inset box area (box 1). The box area (box 2) over the UAE-Oman Mountains is shown in more detail in Figures 10b and c. b) Gravity derived structural trends based on the THDR of residual Bouguer anomaly and location of outer thrust zone as thick black line. c) Magnetic derived structural trends (white denotes maxima or edges) based on the Theta derivative and location of outer thrust zone as thick black line. White dots are principal towns/cities.

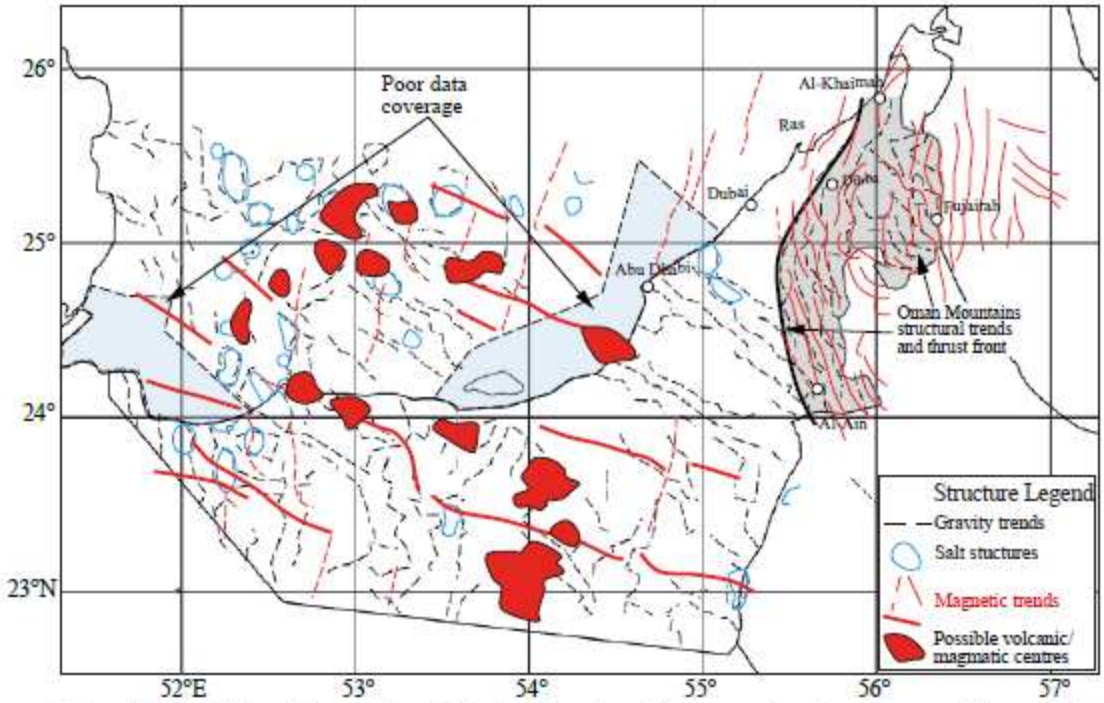

Figure 11. Compilation of structural trends derived from the residual magnetic and gravity maps (Figures 5b, 5c and 9). The outlines of the volcanic/magnetic centres were derived from the THDR of the AS of the DRTP field.

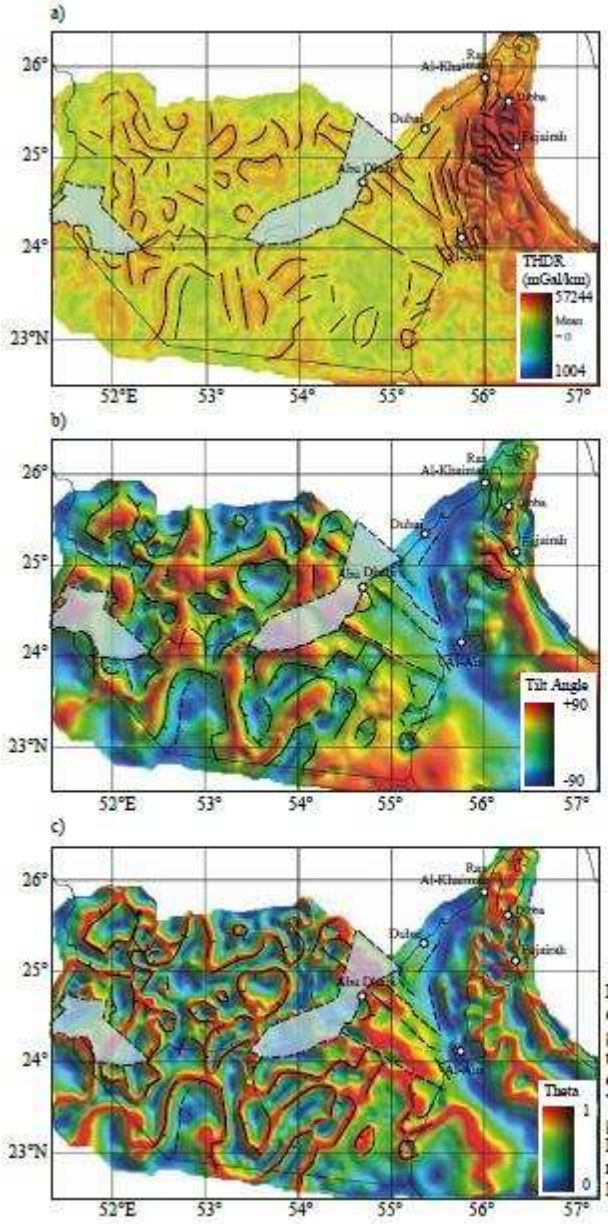

Figure 12. Mapping the intermediate depth structures based on the regional gravity map that images structures in the deep sedimentary section. a) THDR of the regional Bouguer anomaly, b) Tilt angle of the regional Bouguer gravity and c) Theta of the regional Bouguer anomaly. Solid black lines represent edges and tick marks indicate lower density side of the edge structures.

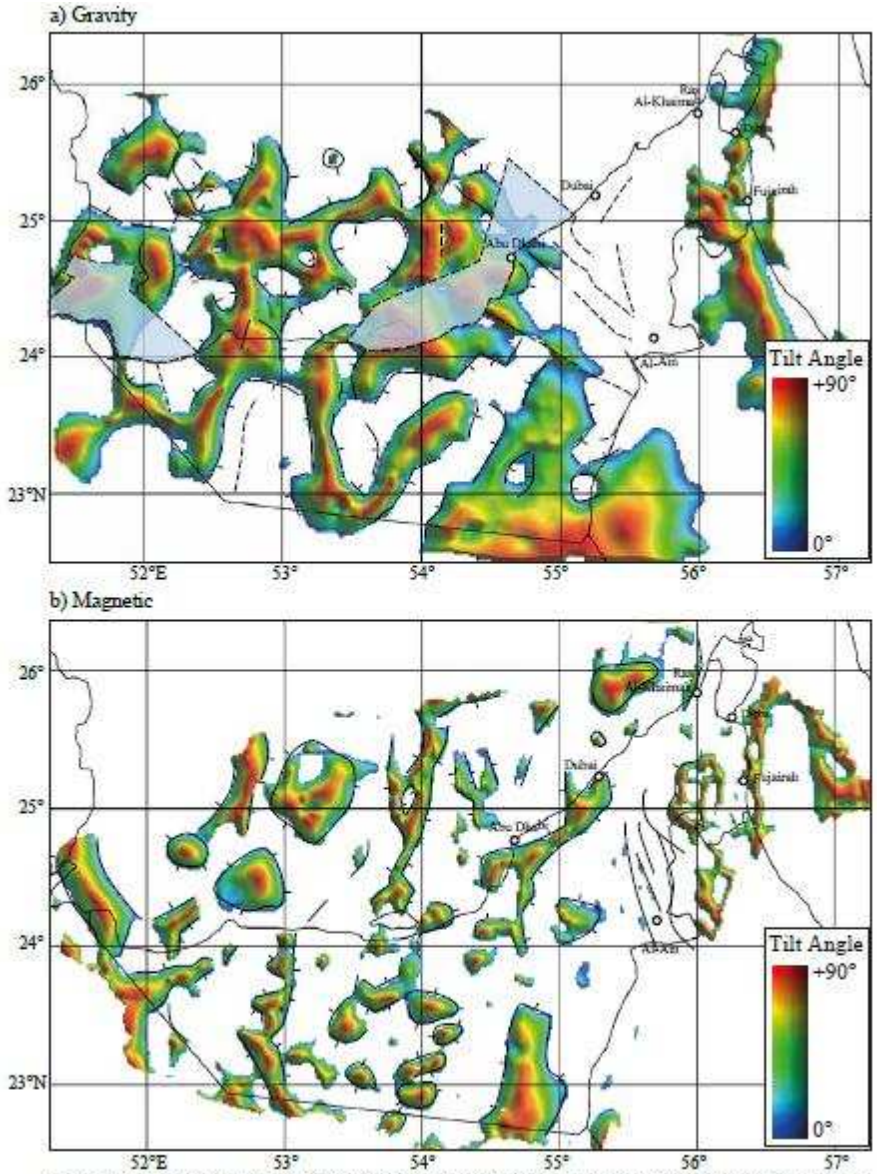

Figure 13. a) Similar to Figure 12b showing the intermediate depth structures based on the regional gravity map that images structural trends in both the deep sedimentary section and basement but now superimposed only on the positive component of the Tilt angle. b) Basement structure trends (faults and contacts) based on the interpretation of the regional magnetic anomaly map superimposed on the positive Tilt angle of the magnetic anomaly (i.e. $\theta > 0.0$). Tick marks indicate lower susceptibility side of the edge structures.

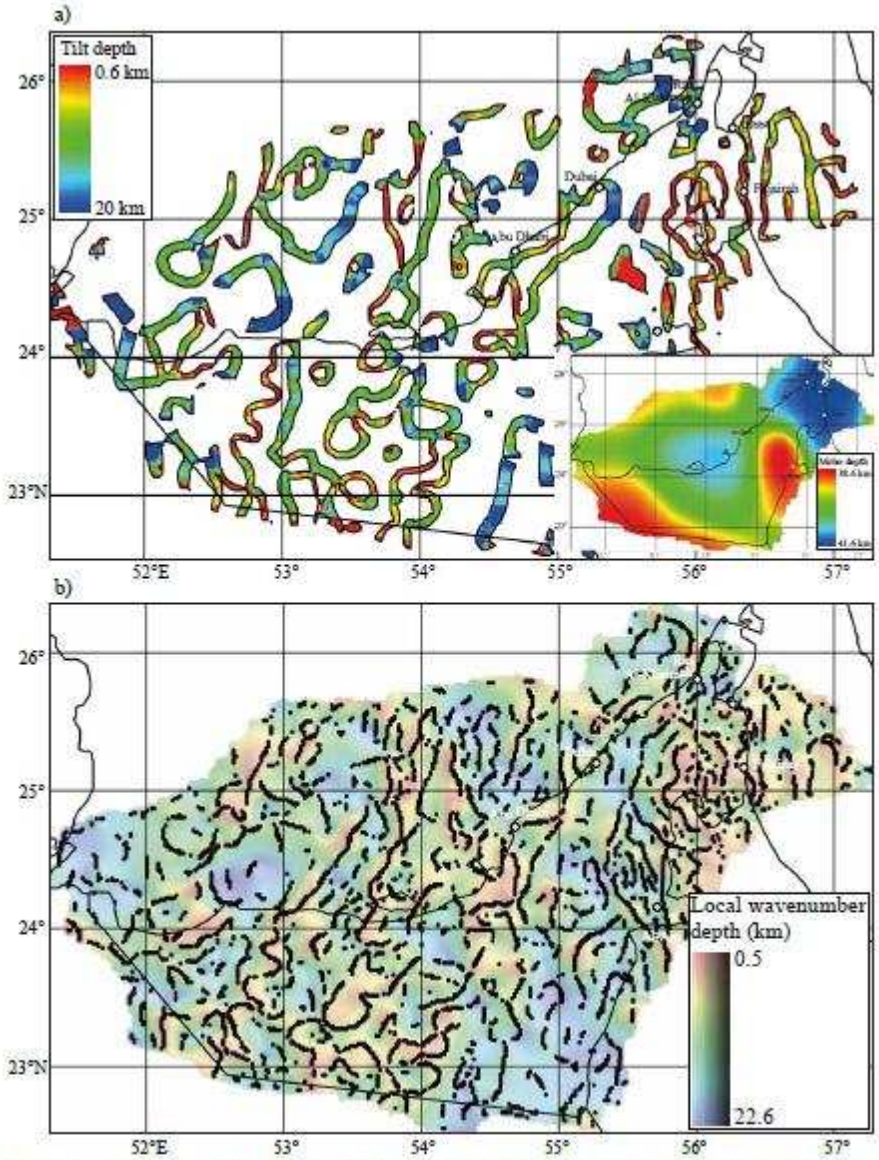

Figure 14. a) Finite tilt-depth plot of the regional magnetic field derived from 20 km low pass filtered magnetic grid and Crust 1.0 Moho model (inset) as a proxy for the depth of the Curie isotherm. The colour depth legend is defined by the width of the Tilt angle contours in the range +/- 25°. b) Finite local wavenumber method depth estimates after Phillips (2000) expanded by minimum curvature gridding to cover the whole of the study area. Black dots are the maxima of the local wavenumber grid and represent the points at which the depth was initially estimated.

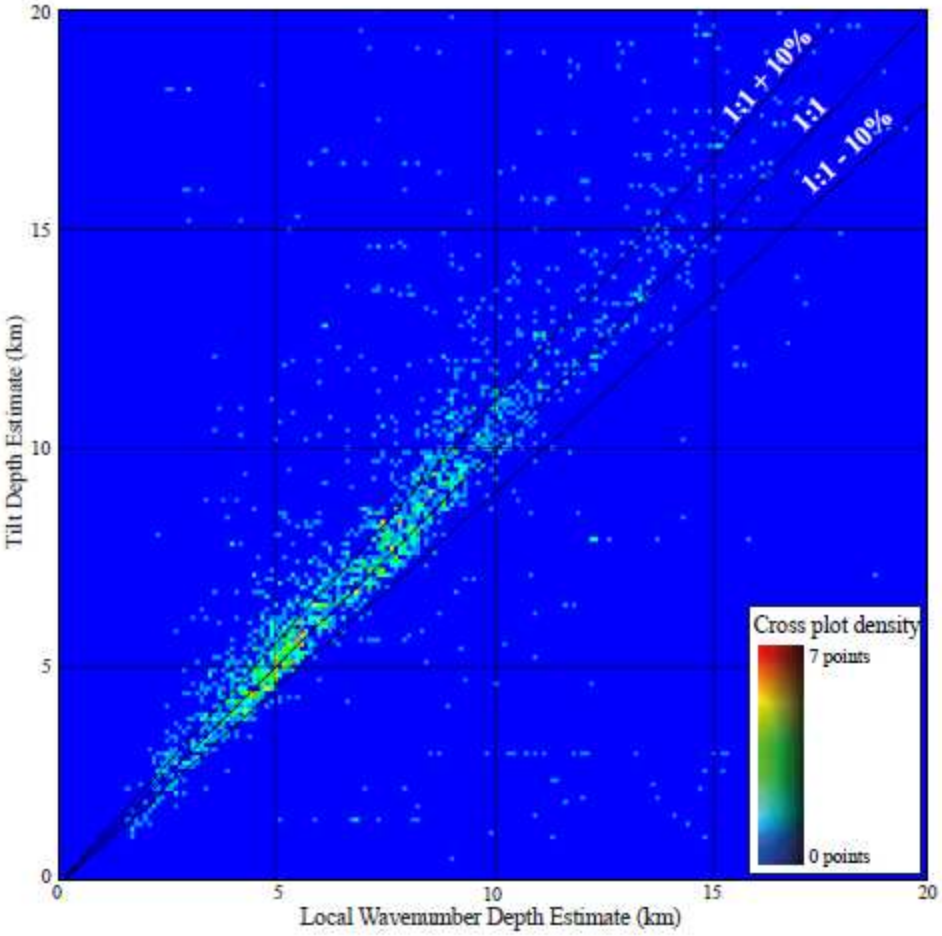

Figure 15. Cross-plot of finite tilt-depth against gridded finite local wavenumber depth estimates, both based on the 20 km low pass filtered DRTP data set. Colours represent density of points. Solutions that lie within the depth range of +/- 10% of each other are used to generate the final depth map (Figure 16).

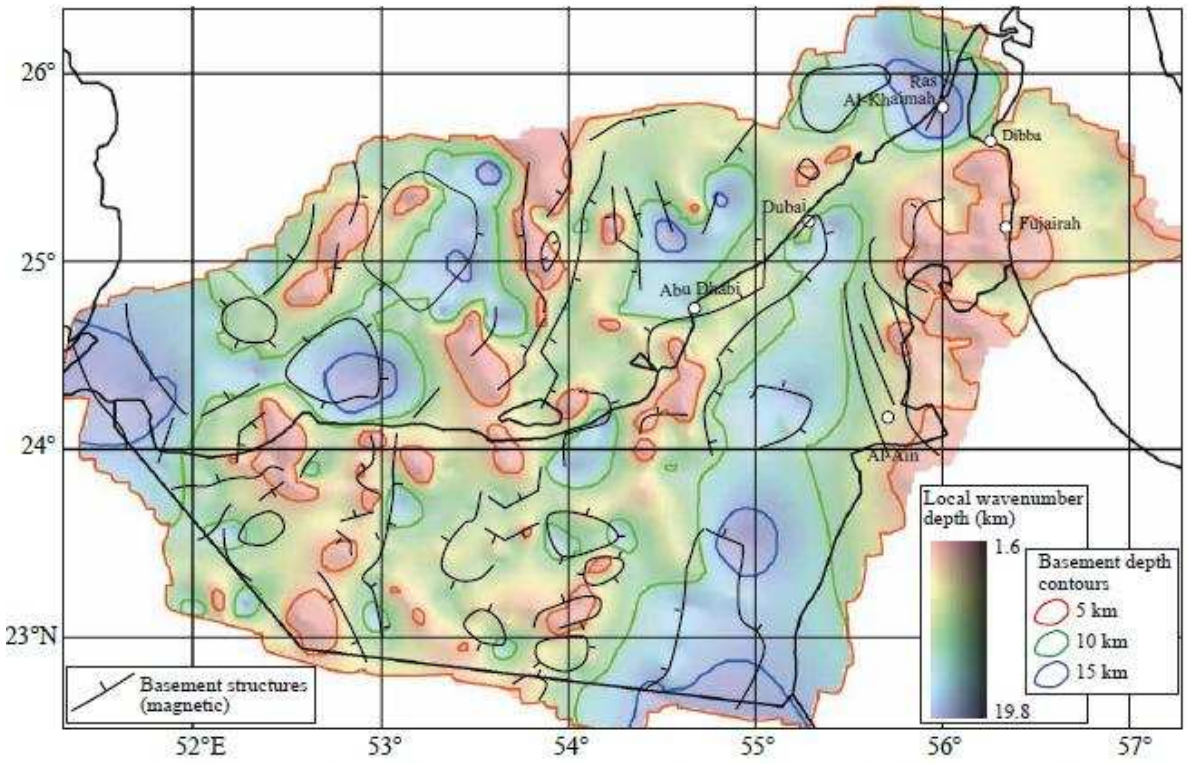

Figure 16. Basement structure and depth map based on finite local wavenumber depth estimates which are within 10% tolerance of the finite tilt depth estimate at the same point. Overlay shows basement structural elements shown in Figure 13b.

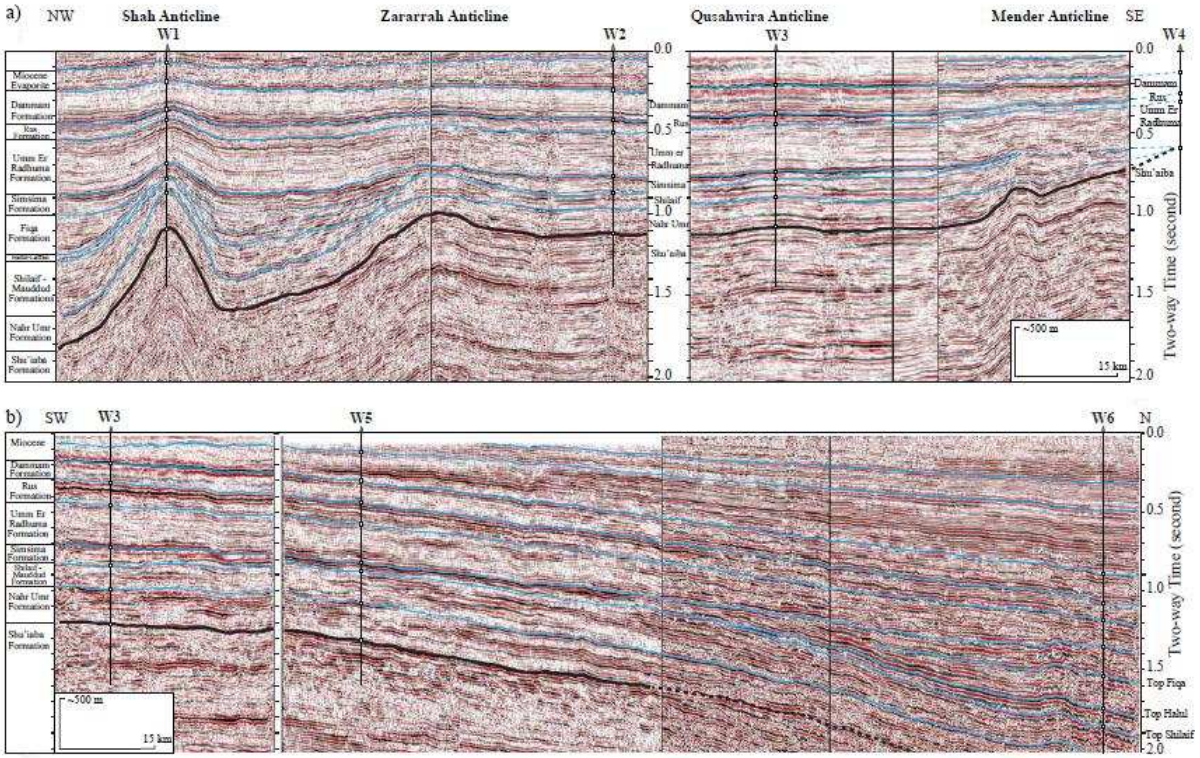

Figure 17. a) NW-SE oriented composite seismic profiles over the Shah, Zararrah, Qusahwira and Mender anticlines. See Figure 1 for locations. Thick black line represents top of Shu'iaba Formation. b) SW-NE oriented composite seismic profiles over the south eastern region of UAE. See Figure 1 for locations. Thick black line represents top of Shu'iaba Formation.

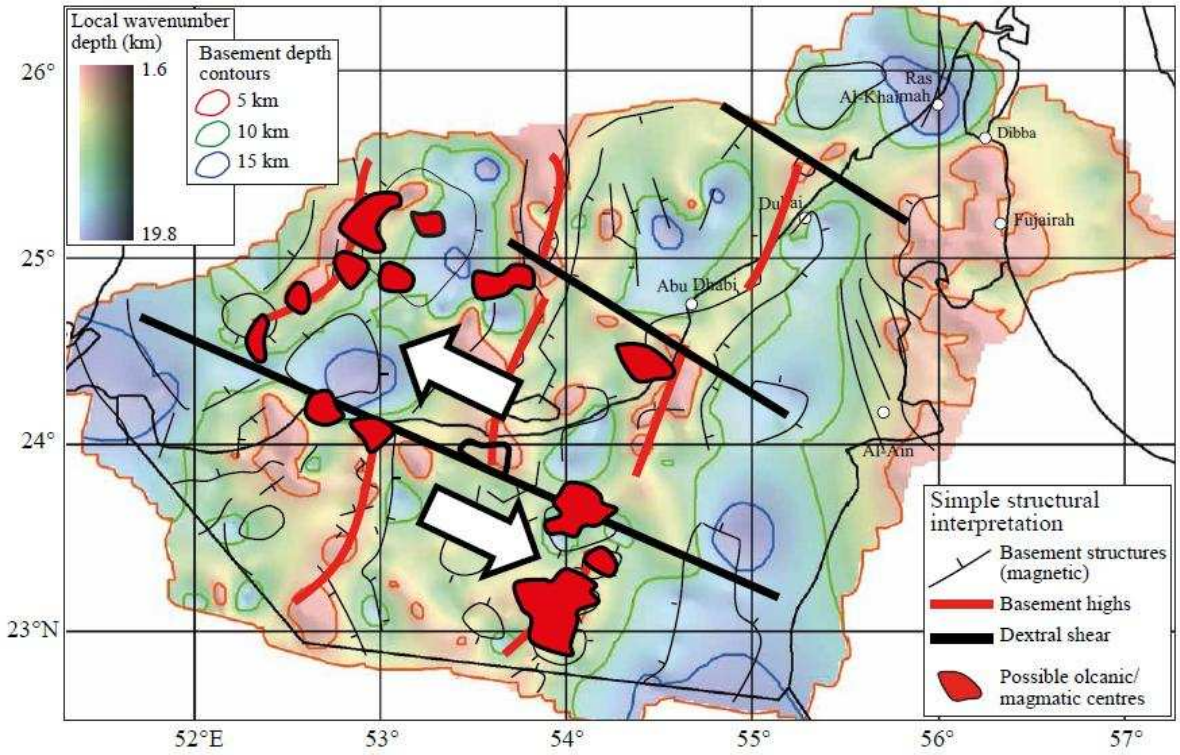

Figure 18. Schematic tectonic map of the UAE. The map highlights basement ridges in bold red lines and positions a WNW-ESE dextral shear structure between the offsets of similar direction as seen in the residual magnetic data but whose location is midway between the two main shears seen in the south-east of the UAE. Superimposed on the simple tectonic map are the main volcanic/magmatic centres.

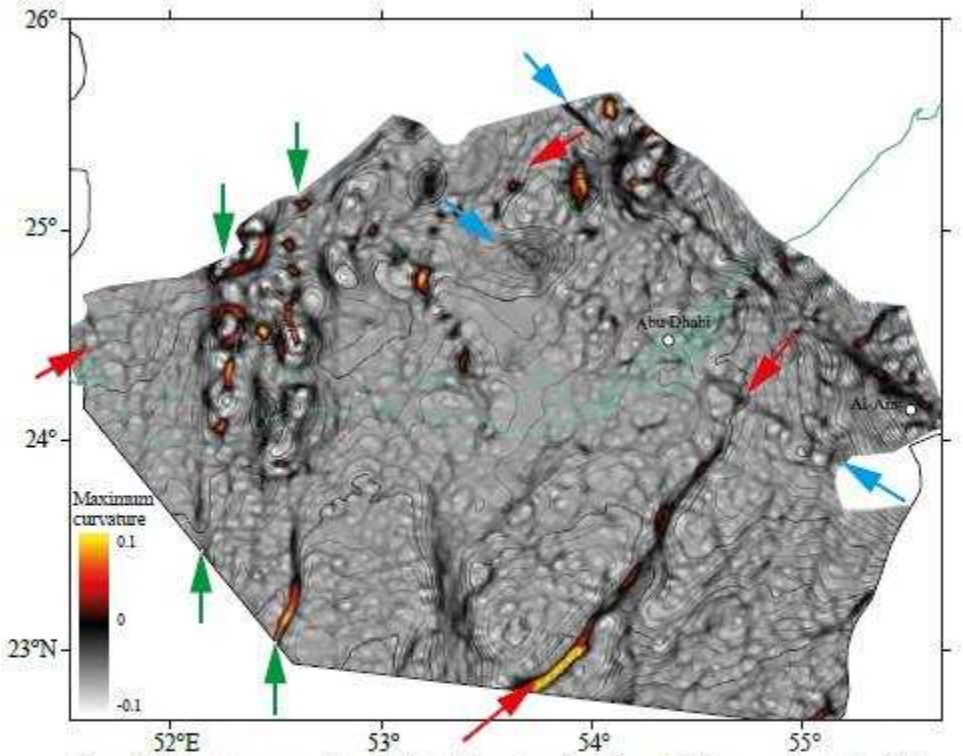

Figure 19 Curvature map of top Shu'iaba Formation (see Figure 17 for approximate depth) in Abu Dhabi emirate showing the main fault system in the area. The map was generated from large 3D and 2D seismic data sets in Abu Dhabi. The map shows major lineaments in the sedimentary cover. Green arrows indicate the N-S and NNW-SSE trending faults; blue arrows show NW-SE trending faults, and red arrow depict the NE-SW trending faults.

Highlights

- Both shallow (~1 km) and deeper (5-15 km) structures were identified in the UAE.
- Residual gravity data delineate salt diapirs and a series of 2D linear structures trending NW-SE.
- Regional magnetic data reveals a set of NNE-SSW trending ridges ~5 km depth with dextral offset.
- Tectonic map links the basement trends, volcanic centres and the location of the main oil fields.